# A critical review on the electrosorption of organic compounds in aqueous effluent -Influencing factors and engineering considerations

Amina Lissaneddine, Marie-Noëlle Pons, Faissal Aziz, Naaila Ouazzani, Laila Mandi, Emmanuel Mousset

# A critical review on the electrosorption of organic compounds in aqueous effluent – Influencing factors and engineering considerations

Amina Lissaneddine[1,2,3], Marie-Noëlle Pons[1], Faissal Aziz[2,3], Naaila Ouazzani[2,3], Laila Mandi[2,3], Emmanuel Mousset[1,*]

[1] *Université de Lorraine, CNRS, LRGP, F-54000 Nancy, France*

[2] *National Center for Research and Studies on Water and Energy (CNEREE), Cadi Ayyad University, B. 511, 40000, Marrakech, Morocco*

[3] *Laboratory of Water, Biodiversity, and Climate Change, Faculty of Sciences Semlalia, Cadi Ayyad University, B.P. 2390, 40000, Marrakech, Morocco*

**VERSION ACCEPTED IN**

***ENVIRONMENTAL RESEARCH* JOURNAL**

**2022**

**IN SPECIAL ISSUE: *"ADVANCED ELECTROCHEMICAL TREATMENTS FOR WATER AND WASTEWATER DECONTAMINATION"***

*Contact of corresponding author: emmanuel.mousset@univ-lorraine.fr

## Abstract

Despite being an old process from the end of the 19$^{th}$ century, electrosorption has attracted renewed attention in recent years because of its unique properties and advantages compared to other separation technologies and due to the concomitant development of new porous electrode materials. Electrosorption offer the advantage to separate the pollutants from wastewater with the possibility of selectively adsorbing and desorbing the targeted compounds. A comprehensive review of electrosorption is provided with particular attention given to the electrosorption of organic compounds, unlike existing capacitive deionization review papers that only focus on inorganic salts. The background and principle of electrosorption are first presented, while the influence of the main parameters (e.g., electrode materials, electrode potential, physico-chemistry of the electrolyte solutions, type of compounds, co-sorption effect, reactor design, etc.) is then detailed and the modeling and engineering aspects are discussed. Finally, the main output and future prospects about recovery studies and combination between electro-sorption/desorption and degradation processes are given.

This review particularly highlights that carbon-based materials have been mostly employed (85% of studies) as porous electrode in organics electrosorption, while existing studies lack of electrode stability and durability tests in real conditions. These electrodes have been implemented in a fixed-bed reactor design most of the time (43% of studies) due to enhanced mass transport. Moreover, the electrode potential is a major criterion: it should be applied in the non-faradaic domain otherwise unwanted reactions can easily occur, especially the corrosion of carbon from 0.21 V/standard hydrogen electrode or the water oxidation/reduction. Furthermore, there is lack of studies performed with actual effluents and without addition of supporting electrolyte, which is crucial for testing the real efficiency of the process. The associated predictive model will be required by considering the matrix effect

along with transport phenomena and physico-chemical characteristics of targeted organic compounds.

**Keywords:** electric double layer, modeling, organic pollutant, reactor design, three-dimensional electrode, wastewater

# Contents

## List of abbreviations and symbols

| Abbreviation | Definition |
|---|---|
| 3D | three-dimensional |
| AC | activated carbon |
| AC-Am | ammonia treated |
| ACC | activated carbon cloth |
| ACCO | oxidized activated carbon cloth |
| ACE | activated carbon electrode |
| ACF | activated carbon fibers |
| AC-HT | annealed activated carbon |
| AC-NA | nitric acid oxidized activated carbon |
| AC-NM | nonmodified activated carbon |
| AO7 | acid orange 7 |
| AO8 | acid orange 8 |
| AR151 | acid red 151 |
| AY14 | acid yellow 14 |
| BA | benzoic acid |
| CB-W | carbon black |
| CFP | carbon fiber paper |
| CNT-c | multiwalled carbon nanotubes - short carboxyl |
| CNT-h | multiwalled carbon nanotubes - short hydroxyl |
| CNTs | carbon nanotubes |
| DFT | density functional theory |
| EDL | electric double layer |
| GAC | granular activated carbon |
| IHP | inner Helmholtz plane |
| MB | methylene blue |
| MSE | mercury/mercurous sulfate electrode |
| MWCNTs | multiwalled carbon nanotubes |
| NA | nicotinic acid |
| NHE | normal hydrogen electrode |
| NMO | $Na_{0.7}MnO_2$ |
| OC | open circuit |
| OHP | outer Helmholtz plane |
| prGO | porous reduced graphene oxide |
| RE | regeneration efficiency |
| rGA | reduced graphene oxide aerogel |
| rGA-Cu | Cu nanoparticles loaded rGA |
| rGA-F | F-doped rGA |
| rGA-F/Cu | F and Cu nanoparticles modified rGA |
| rGO | reduced graphene oxide |
| RHE | reversible hydrogen electrode |
| SCE | saturated calomel electrode |
| SEM | scanning electron microscopy |

| | |
|---|---|
| STR | stirred tank reactor |
| SWCNTs | single-walled carbon nanotubes |

83

| Symbol | Definition |
|---|---|
| $A$ | cross-sectional area |
| $a$ | interfacial area per unit void volume |
| $a_0$ | effective radius of the counterions |
| $Bi_m$ | mass transfer Biot number |
| $C$ | differential capacitance |
| $\bar{c}$ | average salt concentration |
| $C_{in}$ | targeted compound concentration in the inlet flow |
| $C_0$ | initial concentration of the pollutant |
| $C_{bulk}$ | average bulk number density of cations or anions |
| $C_D$ | linear Gouy-Chapmann or Debye capacitance |
| $C_{dc}$ | double-cylinder capacitance for mesopores |
| $C_{dl}$ | double layer specific capacitance |
| $C_e$ | equilibrium concentration of the pollutant |
| $C_{GC}$ | Gouy-Chapman specific capacitance |
| $C_H$ | Helmholtz specific capacitance |
| $C_K$ | diffuse layer capacitance |
| $c_{max}$ | maximal possible local concentration of cations and anions |
| $C_{out}$ | targeted compound concentration in the outlet flow |
| $C_{st}$ | sandwich-type capacitance for micropores |
| $D$ | diffusion coefficient of the targeted compound |
| $d$ | electrode thickness |
| $D_e$ | effective diffusivity |
| $d_{eff}$ | effective separation between the electrode surface and the counterions |
| $D_m$ | molecular diffusivity of pollutant |
| $d_p$ | particle diameter |
| $e$ | elementary charge |
| $G$ | dimensionless time constant representing competition between electrical potential wave and sorption wave |
| $H$ | bed height |
| $j$ | current density |
| $k_B$ | Boltzmann constant |
| $k_f$ | external mass transfer coefficient |
| $L$ | characteristic length |
| $L_0$ | distance between two parallel electrodes having the same polarity |
| $L_D$ | Debye length |
| $m$ | mass of the working electrode |
| $q_A$ | electrosorption capacity |
| $q_D$ | electrodesorption capacity |
| $Q_V$ | inlet flow rate |
| $R_1$ | outer radii of the cylinder |

| | |
|---|---|
| $R_2$ | inner radii of the cylinder |
| $Re$ | Reynolds number |
| $R_f$ | faradaic resistance of the electrochemical reaction |
| $R_s$ | difference in the resistance of the solution between two points of interest in the system |
| $S_{BET}$ | specific surface area estimated by the Brunauer-Emmett-Teller method |
| $Sc$ | Schmidt number |
| $Sh$ | Sherwood number |
| $sr$ | scan rate |
| $T$ | dimensionless time |
| $t$ | reaction time |
| $T_0$ | absolute temperature |
| $t_{dl}$ | double layer charging time |
| $t_{sc}$ | scan time |
| $t_{st}$ | stoichiometric time of sorption |
| $t_{t0}$ | turnover time |
| $U$ | total potential drop across the double layer |
| $u$ | linear velocity of the liquid through the void space of the adsorbent |
| $V$ | volume of solution |
| $V_{me}$ | volume of mesopore |
| $W$ | bed width |
| $Wa$ | Wagner number |

**Greek letters**

| | |
|---|---|
| $\gamma$ | ratio of the average salt concentration |
| $\delta_a$ | diffusion layer thickness at anode |
| $\delta_c$ | diffusion layer thickness at cathode |
| $\Delta E$ | potential difference |
| $\Delta H_{ads}$ | enthalpy of adsorption |
| $\varepsilon_B$ | bed porosity |
| $\varepsilon_f$ | high frequency dielectric constant |
| $\varepsilon_0$ | permittivity of vacuum |
| $\varepsilon_r$ | electrolyte dielectric constant |
| $\eta$ | overpotential |
| $\kappa$ | effective electrolyte conductivity |
| $\nu$ | kinematic viscosity of the solution |
| $\rho_B$ | bed density |
| $\sigma$ | electrical conductivity of the porous material |
| $\psi$ | dimensionless potential |

# 1. Introduction

In recent decades, the increasing industrial expansion and domestic activities has produced significant volumes of wastewater containing undesirable toxic contaminants (e.g., fine suspended solids, metals, organic and inorganic particles, and other impurities). Water pollution is therefore becoming a serious concern in the environmental field (Bagheri et al., 2020; Crini et al., 2019; Crini and Lichtfouse, 2019; Li et al., 2020), and the demand for freshwater represents one of the most critical global challenges of the 21$^{st}$ century (Zhang et al., 2018a). The United Nations Educational, Scientific and Cultural Organization (UNESCO) approximates that nearly over 2 billion people live in countries experiencing high water stress, and this water stress tends to be globalized (UNESCO, 2019). Hence, the interest in wastewater reuse as an alternative resource that can be used for different purposes is arousing strong interest worldwide. Wastewater reclamation and reuse practice is expected to achieve a circular economy approach (Nan et al., 2020). In this context, the implementation of reliable treatments adapted to each type of wastewater and to regulations before reuse is necessary. The application of bioprocesses has been established as a common practice for wastewater treatment when it remains reliable. Although they are inexpensive treatments, their efficiency toward biorecalcitrant pollutants is limited (Ganzenko et al., 2014; Mousset et al., 2021b). Studies on wastewater treatment strategies are performed to define the best wastewater treatment train for application (Rizzo et al., 2020). To satisfy this demand, nonbiological treatments are required (Mousset et al., 2021a; Oller et al., 2011; Rizzo et al., 2020). Various separation techniques have been proposed to remove pollutants from aqueous effluents (Rezakazemi et al., 2018; Rizzo et al., 2020), which mainly consist of physical (i.e., flotation, adsorption, membrane filtration), chemical (i.e., neutralization, coagulation, flocculation, precipitation), and physico-chemical (i.e., electrosorption) technologies (Rezakazemi et al., 2018; Zhang et al., 2017). Among these processes, electrosorption offers many advantages, such as a high removal efficiency (i.e., a high adsorption capacity), fast adsorption kinetics,

and the possibility to control the selectivity and the sorption/desorption steps (Gao et al., 2019; Han et al., 2006a; Rong and Xien, 2009). It is particularly suitable for removing charged and/or polar pollutants by polarizing high surface area electrodes at a given electric current or potential (Bayram et al., 2018; Nainamalai et al., 2018). Contaminants such as pesticides, dyes and solvents have proven to be effectively removed by electrosorption (Bayram et al., 2018; Niu and Conway, 2003; Sahin et al., 2020).

Several general reviews have compiled the different separation techniques used for aqueous effluents, but sections devoted to electrosorption were either minor or nonexistent (Ahmad et al., 2020; Wadhawan et al., 2020). Nevertheless, few reviews have addressed the electrosorption process (Foo and Hameed, 2009; Su and Hatton, 2016). A state-of-the-art review was published on electrosorption technology, its background studies, fundamental chemistry, working principles and the recent development of the activated carbon (AC)-assisted electrosorption process (Foo and Hameed, 2009). In another review, the major classes of separations utilizing electrosorption were presented, and an overview of the progress in materials chemistry was given (Su and Hatton, 2017). They emphasized capacitive deionization as a method for removing inorganic salts without involving electron exchange (Su and Hatton, 2017), while other recent reviews focused mainly on capacitive deionization (Folaranmi et al., 2020; Vafakhah et al., 2020; Volfkovich, 2020; Zhang et al., 2018a). However, to the best of our knowledge, there is no detailed review on the electrosorption of organics as either ionic or nonionic forms. In addition, evaluating the parameters (including engineering factors) that control the electrosorption efficiency is usually not scrutinized. Therefore, we propose focusing on these aspects by enlarging the study from AC to all types of conductive adsorbent materials.

Thus, this review begins by exposing the background and principle of electrosorption technology. The influence of parameters, such as electrode materials, current density,

physico-chemistry of electrolytes and reactor design, is then addressed. Next, the identification of the main influencing factors combined with electrosorption modeling allows the design strategies for implementing porous electrodes to be defined. Finally, future directions for electrosorption processes are presented, which could bring new opportunities for their optimization and future development.

# 2. Electrosorption: background and principle

## 2.1. General background

Electrosorption is the result of the concomitant development of porous electrode materials and electric double layer (EDL) theory.

This is missed most of the time in the literature, but the first hybrid electrochemical method combined with a separation technique using a porous electrode material was proposed as early as the late $19^{th}$ century (1893) by Paul Leon Hulin, who referred to it as the "electroly-filtration" process (Cœuret, 1993; Hulin, 1893). Afterwards, Butler and Armstrong measured hydrogen adsorption on solid metal electrodes in 1933 by applying anodic galvanostatic transients (Butler and Armstrong, 1933; Gileadi et al., 1968). Grahame then studied the potential controlled adsorption of n-octanol in 1946 (Grahame, 1946). This was followed by the development of electrosorption of neutral organic molecules in 1965 (Brummer et al., 1965). During the end of the 1960s and the beginning of the 1970s, granular electrodes were developed (Coeuret, 2003). Porous AC bed electrodes were introduced by Johnson and Newman in 1971 for desalination applications (Johnson and Newman, 1971). From the middle of the 1970s, expanded metal electrodes have aroused particular attention for their easy fabrication and implementation at the industrial scale (Coeuret, 2003; Coeuret and Legrand, 1985). Metal foam electrodes then emerged in the 1980s due to their much higher specific surface area, which is particularly efficient for electrosorption in diluted media (Marracino et al., 1987). Still aimed at increasing the surface area of electrodes,

nanostructured materials emerged in the 2000s, such as carbon nanotubes (CNTs) and graphene (Chabot et al., 2014; Du et al., 2021; Huong Le et al., 2019). Metal organic framework (MOF)-based materials have been proposed more recently for electrosorption due to their exceptional surface area with controllable porosity (Chang et al., 2015).

In the meantime, the understanding of the EDL mechanism aroused specific attention within the electrochemistry community. It began with studies about the potential drops at the electrode/electrolyte interface and the so-called "Volta problem". Many known scientists have attempted to explain this phenomenon, such as Volta, Nernst, Ostwald, Planck, Langmuir and Lorenz (Damaskin and Petrii, 2011). Several EDL theories have been developed (Pilon et al., 2015), mainly through phenomenological models that could be supported by experimental data obtained by two kinds of electrochemical techniques: (i) electrocapillary curves, first developed by Lippmann (Lippmann, 1875) and (ii) EDL differential capacitance plots, first proposed by Varley (Varley, 1871). Helmholtz was the first to formalize the EDL concept in 1879 (Helmholtz, 1879), suggesting the existence of a compact layer made of a monolayer of counterions inducing a linear decrease in the potential in the vicinity of an oppositely charged conductive surface (Helmholtz, 1879). In contrast to the assumption of a continuous distribution of ions in the electrolyte upon the Poisson-Boltzmann relation at thermodynamic equilibrium, Gouy (Gouy, 1910) and Chapman (Chapman, 1913) proposed an alternative in the 1910s, introducing the existence of a diffuse double layer, which induces a nonlinear decrease in the potential in the vicinity of the electrode. The Gouy-Chapman approach was still not convincing at the closest distance of the electrode. The ion concentration was overestimated at the electrode surface because the ions were taken as point charges instead of having a finite size. Thus, in 1924 Stern proposed juxtaposing both the Helmholtz and Gouy-Chapman models (Stern, 1924), in which the EDL is composed of a compact layer close to the surface of the electrode and a diffuse layer in the outer region. In 1947 Grahame proposed dividing the compact layer (i.e., Stern layer) into the inner Helmholtz plane (IHP) and the

outer Helmholtz plane (OHP). The IHP consists of a layer of ions and solvent adsorbed by covalent bonds and/or van der Waals forces on the interface. In the OHP, ions are driven by electromigration effects to produce an ionic environment (Grahame, 1947). Figure 1 schematizes the EDL considering the so-called Gouy-Chapman-Stern model, which includes IHP and OHP (Chapman, 1913; Gouy, 1910; Grahame, 1947; Helmholtz, 1879; Stern, 1924). This polarized interface induces a capacitance whose values usually range between a few µF $cm^{-2}$ to several tens of µF $cm^{-2}$ (Simon and Gogotsi, 2008).

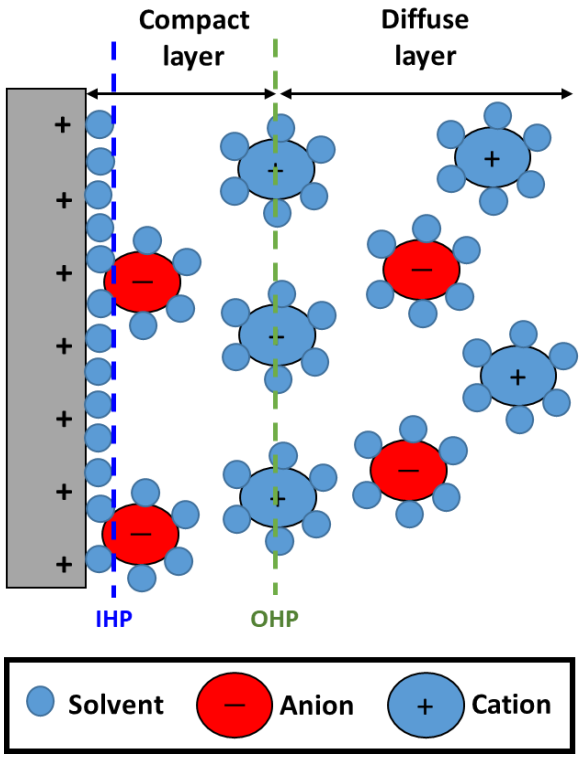


**Fig. 1.** Schematic representation of the EDL at positively charged electrode materials in the presence of anions, cations and solvent.

## 2.2. Principle

Electrosorption is a heterogeneous process that is defined as the species adsorption induced by electric current or a polarization potential on the surface of a conductive material without involving faradaic reactions, i.e., without electron transfer reactions (Fig. 2) (Frumkin et al.,

1974; Gerçel, 2016). The electrosorption efficiency is usually quantified by estimating the equilibrium electrosorption capacity ($q_A$ in mg $g^{-1}$), according to Eq. 1 (Li et al., 2016):

$$q_A = \frac{(C_0 - C_e)\,V}{m} \quad (1)$$

where $C_0$ and $C_e$ are the initial and equilibrium concentrations of the pollutant, respectively (g $L^{-1}$), $V$ is the volume of the solution (L), and $m$ is the mass of the working electrode (g).

The higher the electrosorption capacity is, the higher the electrosorption efficiency is (Alencherry et al., 2017).

The electric potential or current is the third driving force of the electrosorption phenomenon and ion exchange mechanism (Jung et al., 2005), while the transport steps remain essential for the entire process efficiency (Schultze and Vetter, 1973; Vetter and Schultze, 1974). Diffusion (i.e., species subjected to a concentration gradient in the vicinity of the electrode), electromigration (i.e., ions subjected to a gradient of the electrostatic potential) and convection (i.e., global fluid movement in the bulk) phenomena can occur in the electrochemical reactor, which has been formalized by the Nernst-Planck equation (Bard and Faulkner, 2001). Most of the time, diffusion and/or electromigration of organic species in diluted media are limited steps before subsequent electrosorption (Adnan et al., 2021a; Alagesan et al., 2021; Coeuret, 2003; Mousset et al., 2019a; Panizza et al., 2001). Electromigration represents an interesting feature when organic ionic species are present in a solution since it can facilitate their selective transport toward the oppositely charged electrode for electrosorption. Nevertheless, the electrosorption of uncharged organic compounds remains feasible by following replacement reactions at an equivalent volume between water molecules adsorbed on the electrode and the organic compound (Gileadi, 1966).

Apart from transport phenomena, the behavior at the electrode/electrolyte interface is another important concern for efficient electrosorption. This can be characterized by the EDL, which

usually needs to be maximized. EDLs have been shown to depend on electrode material properties (i.e., electronic structure of the metal surface, electrode surface roughness, porosity and pore size distribution), interelectrode distances and electrolyte characteristics (i.e., electrolyte concentration, viscosity and polarity, distribution of ions and solvent molecules) (Conway, 1999; Oleinick et al., 2019; Schmickler, 1996; Trasatti, 1992; Yan et al., 2017). The influence of parameters on the organic electrosorption efficiency is discussed in more detail in section 3.

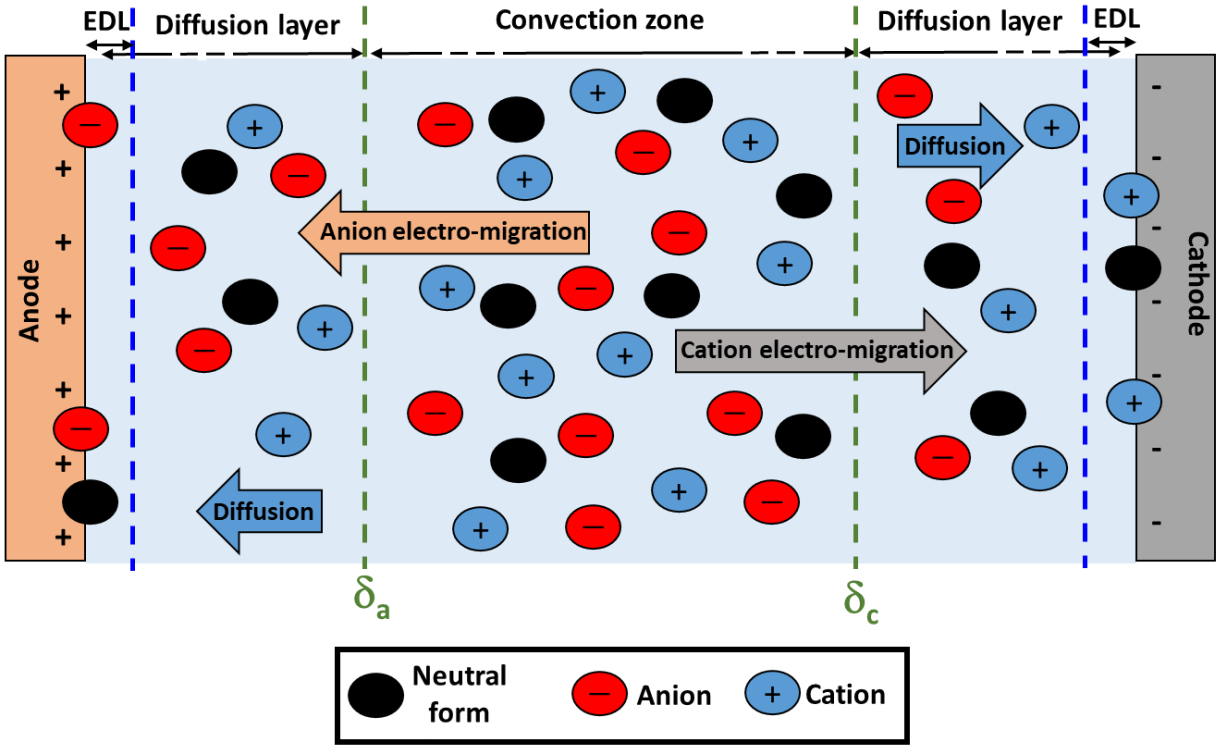


**Fig. 2.** Schematic diagram illustrating the principle of electrosorption, including anion, cation and uncharged compounds, as well as transport phenomena ($\delta_a$ and $\delta_c$: diffusion layer thickness at the anode and cathode, respectively).

## 3. Influence of the main parameters

The effect of the main parameters (i.e., the properties of the electrode materials, the experimental conditions (applied electrode potential, pH, concentration, electric conductivity, residence time, flow rate) and the reactor design) on the electrosorption/desorption kinetics and capacity have been reviewed in detail. The main research articles dealing with electrosorption of organic compounds in the literature are listed in Table 1.

248 **Table 1.** Main studies performed on the electrosorption of organic compounds reviewed in the literature.

| Working electrode | Specific surface area | Reactor design | Organic pollutant (concentration) | Electrolyte (concentration) | Current intensity/Electrode potential | Studied parameters | Maximum electrosorption capacity | Reference |
|---|---|---|---|---|---|---|---|---|
| Granular activated carbon (GAC) | 1180 $m^2 g^{-1}$ | Fixed-bed reactor | Metribuzin (50,150, 300 and 450 mg $L^{-1}$) | KCl (3 mol $L^{-1}$) | −0.050 V/SCE | Electrode potential, flow rate and initial concentration of pollutant | 22 mg $g^{-1}$ | (Kitous et al., 2009) |
| GAC | 950 $m^2 g^{-1}$ | Fixed-bed reactor | Naphthalenesulfonic acid, benzyl alcohol, naphthoic acid, methylquinolinium chloride (2 mg $L^{-1}$) | KCl (0.1 mol $L^{-1}$) | 0.60 V/(Ag/saturated KCl) | Initial concentration of pollutant and pH of the initial solution | 100 mg $g^{-1}$ | (Bán et al., 1998) |
| GAC | - | Fixed-bed reactor | Benzene (1 mmol $L^{-1}$) | KCl (0.2 mol $L^{-1}$) | -2 and 2 V/SCE | Electrode potential | - | (Plaisance et al., 1996) |
| GAC | 1100 $m^2 g^{-1}$ | Fixed-bed reactor | Ethylenediamine (500 mg $L^{-1}$) | NaCl (20 wt. %) and $NaHCO_3$ (0.025 mol $L^{-1}$) | 0 to -1 V/SCE | Initial concentration of pollutant and electrode potential | - | (Eisinger and Keller, 1990) |
| GAC and platinum wire | - | Fixed-bed reactor | Chloroform (2.5-10 mmol $L^{-1}$) | $KNO_3$ (0.1 mol $L^{-1}$) | 0, 1, 2 and 2.5 V/SCE | Electrode potential | - | (Hazourli et al., 1996) |
| GAC and activated carbon electrode (ACE) | GAC: 1062 $m^2 g^{-1}$ ACE: 862 $m^2 g^{-1}$ | Flow-through parallel-plate cell | Benzoic acid (BA) and nicotinic acid (NA) (1 mmol $L^{-1}$) | $Na_2SO_4$ (0.1 mol $L^{-1}$) | 0.5, 1.5 and 2 V/(Ag/AgCl) | Time, flow rate and electrode potential | - | (Bayram, 2016) |
| Activated carbon cloth (ACC) | 1870 $m^2 g^{-1}$ | Flow-through parallel-plate cell | BA (0.22 mmol $L^{-1}$) | $Na_2SO_4$ (0.01 mol $L^{-1}$) | 0.60 V/(Ag/AgCl) | Flow rate, electrode potential and pH of initial solution | 180 mg $g^{-1}$ | (Bayram and Ayranci, 2012a) |

| | | | | | | | | |
|---|---|---|---|---|---|---|---|---|
| ACC | ACC:926 $m^2 g^{-1}$ ACCO: 960 $m^2 g^{-1}$ | Flow-through parallel-plate cell | Bentazone (20 mg $L^{-1}$) | $Na_2SO_4$ (0.01 mol $L^{-1}$) | 5 mA | Time, initial concentration of pollutant, pH of the initial solution | ACC: 127 mg $g^{-1}$ ACCO: 57 mg $g^{-1}$ | (Ania and Béguin, 2007) |
| ACC | 1870 $m^2 g^{-1}$ | STR | Acid orange 8 (AO8), acid yellow 14 (AY14), and acid red 151 (AR151) (0.05 mmol $L^{-1}$) | $Na_2SO_5$ (0.1 mol $L^{-1}$) | 1 V/(Ag/AgCl) | Time and initial concentration of pollutant | AO8: 20 mg $g^{-1}$ AY14: 25 mg $g^{-1}$ AR151: 24 mg $g^{-1}$ | (Sahin et al., 2020) |
| ACC | 1870 $m^2 g^{-1}$ | Flow-through parallel-plate cell | 2,4-dichlorofenoxy-acetic acid (0.2 mmol $L^{-1}$) | $Na_2SO_4$ (0.01 mol $L^{-1}$) | 0.90 V/(Ag/AgCl) | Flow rate, electrode potential, and electrolyte concentration | 729 mg $g^{-1}$ | (Bayram et al., 2018) |
| ACC | 1186 $m^2 g^{-1}$ | Flow-through parallel-plate cell | Mercury (II) acetate | NaCl (0.01 mol $L^{-1}$) | −1 V/SCE | Flow rate, initial concentration of pollutant, electrode potential and pH of the initial solution | 637 mg $g^{-1}$ | (Jayson et al., 1987) |
| ACC | 596 $m^2 g^{-1}$ | Fluidized-bed reactor | 8-quinolinecarboxylic acid (50 mg $L^{-1}$) | $Na_2SO_4$ (0.5 mol $L^{-1}$) | 3 V (cell potential) | Time and cell potential | 24 mg $g^{-1}$ | (López-Bernabeu et al., 2016) |
| ACC | 2500 $m^2 g^{-1}$ | Flow-through parallel-plate cell | Aniline and pyridine | $LiClO_4$ (0.1 mol $L^{-1}$) | 0.1, 0.2 and 0.4 V/(Ag/AgO) | Electrode potential | - | (Niu and Conway, 2003) |
| AC bed and platinum wire | - | Fixed-bed reactor | Phenol (0 to 100 mg $L^{-1}$) | $Na_2SO_4$ (0.5 mol $L^{-1}$) | - 0.60 V/SCE | Time, initial concentration of the pollutant and electrode potential | - | (McGuire et al., 1985) |

| | | | | | | | | |
|---|---|---|---|---|---|---|---|---|
| Powdered carbon bed | AC-NM: 1390 $m^2$ $g^{-1}$<br>AC-NA: 1296 $m^2$ $g^{-1}$<br>AC-Am: 1212 $m^2$ $g^{-1}$<br>AC-HT:363 $m^2$ $g^{-1}$<br>CB-W: 227 $m^2$ $g^{-1}$<br>CNT-h: 156 $m^2$ $g^{-1}$<br>CNT-c: 209 $m^2$ $g^{-1}$ | Fixed-bed reactor | 4-chlorophenols (10, 25, 50 mmol $L^{-1}$) | $Na_2SO_4$ (0.1 mol $L^{-1}$) | 0.4 V/SCE | Electrode potential and initial concentration of the pollutant | - | (Biniak et al., 2013) |
| AC | 678 $m^2$ $g^{-1}$ | Fluidized-bed reactor | Burdem orange II (30 and 100 mg $L^{-1}$) | $Na_2SO_4$ and $NaNO_3$ (5 mg $L^{-1}$) | 50, 75 and 100 V (cell potential) | pH of the initial solution, initial concentration of pollutant, flow rate, cell potential, and electrolyte concentration | 179 mg $g^{-1}$ | (Gerçel, 2016) |
| AC –perlite mixture (8:1) | - | Fixed-bed reactor | Acilan blau dye (30, 40 and 100 mg $L^{-1}$) | NaCl (0.1 and 0.3 mol $L^{-1}$) | 5, 10, 15 and 20 V (cell potential) | Initial concentration of the pollutant, bed height, cell potential, flow rate, and electrolyte concentration | 17 mg $g^{-1}$ | (Koparal et al., 2002) |
| Carbon bed and the platinum mesh screen | 1010 $m^2$ $g^{-1}$ | Fixed-bed reactor | Pentanol and heptanol (0.01, 0.02, 0.1 mol $L^{-1}$) | $Na_2SO_4$ (1 mol $L^{-1}$) ) | -0.65 V to -0.20 V/($Hg/Hg_2SO_4$ in 1 M $H_2S0_4$) | Electrode potential and initial concentration of the pollutant | - | (Zabasajja and Savinell, 1989) |
| Graphite powder | 0.048 $m^2$ $g^{-1}$ | Fixed-bed reactor | β-naphthol (1 mmol $L^{-1}$) | $K_2SO_4$ (0.5 mol $L^{-1}$) | -0.17, -0.27, -0.50, -0.76, -1.12 and -1.44 V/MSE | Time, initial concentration of the pollutant and electrode potential | - | (Eisinger and Alkire, 1980) |

| | | | | | | | | |
|---|---|---|---|---|---|---|---|---|
| Porous Vycor glass tubing packed with graphite particles | - | Fixed-bed reactor | Quinones (0.1 mmol $L^{-1}$) | KCl (0.1 mol $L^{-1}$) | 1 V/(Ag/AgCl) | Initial concentration of the pollutant and cell potential | - | (Strohl and Dunlap, 1972) |
| Activated carbon fibers (ACF) | 1335 $m^2$ $g^{-1}$ | STR | Phenol (0.4, 1, and 2 mmol $L^{-1}$) | $Na_2SO_4$ (0.001, 0.01, and 0.1 mol $L^{-1}$) | 0.70 V/SCE | Electrode potential, initial concentration of the pollutant, temperature and electrolyte concentration | 350 mg $g^{-1}$ | (Han et al., 2006b) |
| ACF | 1335 $m^2$ $g^{-1}$ | STR | Aniline (2 mmol $L^{-1}$) | $Na_2SO_4$ (0.01 mol $L^{-1}$) | 0.60 V/SCE | Electrode potential, electrolyte concentration, temperature and pH of the initial solution | 316 mg $g^{-1}$ | (Han et al., 2006a) |
| ACF connected by platinum wire | 1335 $m^2$ $g^{-1}$ | STR | Acid orange 7 (AO7) (1 mmol $L^{-1}$) | $Na_2SO_4$ (0.01 mol $L^{-1}$) | 0.60 V/SCE | Time, electrode potential and initial concentration of the pollutant | - | (Han et al., 2008) |
| ACF | - | STR | Aniline (0.05 mg $L^{-1}$) | $Na_2SO_4$ (0.01 mol $L^{-1}$) | 0.20 to 0.40 V/SCE | Electrolyte concentration, temperature and pH of the initial solution | - | (Chai et al., 2007) |
| AC felt | 27 $m^2$ $g^{-1}$ | Flow-through parallel-plate cell | Thiocyanate anions (0.1-0.6 mmol $L^{-1}$) | $H_2SO_4$ (0.5 mol $L^{-1}$) | 0.5, 0.8, and 1.2 mA | Electrode potential and pH of the initial solution | 4 mg $g^{-1}$ | (Rong and Xien, 2005) |
| AC felt and Pt wire | 1367 $m^2$ $g^{-1}$ | Flow-through parallel-plate cell | Thiocyanate (0.1-0.2 mmol $L^{-1}$) | $HNO_3$ or NaOH (0.01 mol $L^{-1}$) | 0.5 to 1.2 mA | pH of the initial solution, electrode polarization and current intensity | - | (Rong and Xien, 2009) |

| | | | | | | | | |
|---|---|---|---|---|---|---|---|---|
| Carbon-felt attached to a short Pt wire. | 2500 $m^2 g^{-1}$ | Flow-through parallel-plate cell | Phenol, phenoxide and chlorophenols (1 mmol $L^{-1}$) | $H_2SO_4$ (0.01 mol $L^{-1}$) | 0.6 mA | Time | - | (Ayranci and Conway, 2001) |
| Carbonaceous aerogel honeycomb monolith | 393 $m^2 g^{-1}$ | STR | Diclofenac (150, 300, 600 and 1000 mg $L^{-1}$) | $Na^2SO_4$ (0.005, 0.01 and 0.02 mol $L^{-1}$) | 0.7, 0.9 and 1.1 V (cell potential) | Electrode gap, electrode potential and initial concentration of the electrolyte | 120 mg $g^{-1}$ | (Pazos et al., 2021) |
| Graphene aerogel | 211 $m^2 g^{-1}$ | STR | Acid red 88, orange II, and MB (0.04–0.2 mmol $L^{-1}$) | $Na_2SO_4$ and NaOH (1 mol $L^{-1}$) | 0.6 V | Time, electrode potential and pollutant concentration | acid red 88: 481 mg $g^{-1}$ orange II: 223 mg $g^{-1}$ MB: 191 mg $g^{-1}$ | (Sun et al., 2016) |
| Porous reduced graphene oxide (prGO)/single-walled carbon nanotubes (SWCNTs) | 94 $m^2 g^{-1}$ | STR | Methylene blue (MB) (10−600 mg $L^{-1}$) | $Na_2SO_4$ (0.01 mol $L^{-1}$) | −1.2 V/(Ag/AgCl) | Time and initial concentration of the pollutant | 13 g $g^{-1}$ | (Yue et al., 2019) |
| Graphene oxide aerogel loaded with Cu nanoparticles and fluorine | GO: 286.75 $m^2 g^{-1}$ rGA:188.92 $m^2 g^{-1}$ F-rGA: 203. $m^2 g^{-1}$ Cu-rGA: 151.65 $m^2 g^{-1}$ Cu/F-rGA: 133.49 $m^2 g^{-1}$ | STR | Perfluorooctanoic acid (1 mg $L^{-1}$) | $Na^2SO_4$ (1-20 mmol $L^{-1}$) | 0 to + 1.6 V/(Ag/AgCl) | pH, temperature, electrode potential and initial concentration of the electrolyte | rGA:6.05 mg $g^{-1}$ rGA-F: 8.43 mg $g^{-1}$ rGA-Cu: 16.47 mg $g^{-1}$ rGA-Cu/F: 25.93 mg $g^{-1}$ | (Liu et al., 2021) |
| Porous MXene/single-walled carbon nanotubes | 42.89 $m^2 g^{-1}$ | STR | MB and methyl orange (30–1000 mg $L^{-1}$) | Phosphate buffer solution (0.01 mol $L^{-1}$) | −2.4 V, −1.2 V, −0.6 V and 0 V/(Ag/AgCl) | Electrode potential, initial concentration of the pollutant and time | 28.4 g $g^{-1}$ | (Yao et al., 2021) |

| | | | | | | | | |
|---|---|---|---|---|---|---|---|---|
| Glassy carbon | - | Fixed-bed reactor | B-naphthol (0.02 mmol $L^{-1}$) | $K_2SO_4$ (0.5 or 0.2 mol $L^{-1}$) | -0.26 V/MSE | Time and initial concentration of the pollutant | - | (Eisinger, 1983) |
| AC and two copper circular plates | - | Fixed-bed reactor | MB (1, 10 and 15 mg $L^{-1}$) | - | 5 V (cell potential) | Bed height, flow rate and initial concentration of the pollutant | 81 mg $g^{-1}$ | (Nainamalai et al., 2018) |
| Pt small spherical of Pt | - | STR | Benzene ($2 \times 10^{-6}$ - $4 \times 10^{-4}$ mol $L^{-1}$) | - | 0.4-0.5 V/RHE | Electrode potential, temperature | - | (Gileadi et al., 1968) |
| Platinum-plated gold | - | STR | Benzene ($2 \times 10^{-6}$ - $4 \times 10^{-4}$ mol $L^{-1}$) | $H_2SO_4$ and $H_3PO_4$ (1 N) | 0.4-0.5 V/NHE | Electrode potential, pH of the initial solution, and time | - | (Heiland et al., 1966) |
| Platinum-plated gold | - | STR | Ethylene | $H_2SO_4$ (1 N) | 0.4-0.46 V/MSE | Electrode potential, initial concentration of the pollutant and temperature | - | (Gileadi et al., 1965) |
| Stainless steel wire coated with monolithic porous polymer micro-column | - | STR | Cresol red (5 mg $L^{-1}$) | NaCl (0.005, 0.5 and 0.1 mg $L^{-1}$) | 0.3 mA | Cell potential, extraction and desorption time, pH of the initial solution and ionic strength | - | (Wang et al., 2012) |

| | | | | | | | | |
|---|---|---|---|---|---|---|---|---|
| Redox polymer polyvinylferrocene /conducting polymer polypyrrole doped with a large anionic surfactant | - | Flow-through parallel-plate cell | Benzoate (0.25 mmol $L^{-1}$) | $NaClO_4$ (12.5 mol $L^{-1}$) | 0.35 V and −0.1 V/(Ag/AgCl) | Electrode potential | - | (He et al., 2020) |

**Abbreviations:** AC: activated carbon; AC-Am: ammonia-treated activated carbon; ACC: activated carbon cloth; ACCO: activated carbon cloth oxidized; ACE: activated carbon electrode; ACF: activated carbon fibers; AC-HT: annealed activated carbon; AC-NA: nitric acid oxidized activated carbon; AC-NM: nonmodified activated carbon; AO7: acid orange 7; AO8: acid orange 8; AR151: acid red 151; AY14: acid yellow 14; BA: benzoic acid; CB-W: carbon black; CFP: carbon fiber paper; CNT-c: multiwalled carbon nanotubes - short carboxyl; CNT-h: multiwalled carbon nanotubes - short hydroxyl; MB: methylene blue; MSE: mercury/mercurous sulfate electrode; NA: nicotinic acid; NHE: normal hydrogen electrode; NMO: $Na_{0.7}MnO_2$; prGO: porous reduced graphene oxide; RHE: reversible hydrogen electrode; rGA: reduced graphene oxide aerogel; rGA-Cu: Cu nanoparticles loaded rGA; rGA-F: F-doped reduced graphene oxide aerogel; rGA-Cu/F: F and Cu nanoparticles modified rGA; SCE: saturated calomel electrode; STR: stirred tank reactor; SWCNTs: single-walled carbon nanotubes.

## 3. 1. Electrode materials

The electrosorption efficiency partly depends on the nature of the electrode materials and their characteristics, i.e., specific surface area, porosity, conductivity, surface functions and surface wettability.

### 3.1.1. Nature and surface morphology of the electrode materials

Various electrode materials have been employed for electrosorption technologies, and Fig. 3a shows the occurrence frequency regarding the electrode materials used in the literature (Table 1). These materials are proposed for classification into the following categories (percentage of occurrence in brackets): carbon-based electrodes (85%), metal-based electrodes (9%) and polymer/resin-based electrodes (6%). Under the carbon electrodes, the following subcategories can be found: carbon-based composites (19%), granular activated carbon (GAC) (32%), carbon cloth (19%), carbon fiber (7%), carbon felt (7%), graphite (13%) and graphene (3%).

Metal-based materials have barely been studied in the literature (Fig. 3a), probably due to their usually high cost compared to carbon materials and their lower flexibility in terms of shape, surface area and porosity. The crystallographic orientation of the single crystal planes (Lust et al., 1997a, 1997b) and the electronic structure of the metal surface impact the EDL, and therefore the electrosorption efficiency (Schmickler, 1996). It has been further demonstrated that the dipole orientation of water, often used as a solvent, can be impacted by the surface chemistry of metal-based materials (Conway, 1999). The point of zero charge of metals influences the specific orientation of $H_2O$ molecules, which then impacts $H_2O$ adsorbability (Trasatti, 1972). Therefore, the adsorbability of solvated ions on metals is also impacted, along with their electrosorption efficiency.

In contrast, it is obvious that carbon represents the majority of electrode materials used in the literature (Fig. 3a). Despite their availability and low prices, this enthusiasm toward carbon

materials can be explained by their adequate properties for electrosorption, which are discussed more in detail in sections 3.1.2 to 3.1.5. Among their important characteristics, they have a particularly high surface area, high porosity, high electrical conductivity and high electrochemical stability, especially for cathodic reduction (Frackowiak, 2001; Hou et al., 2012). Graphene has notably attracted attention as an emerging two-dimensional material composed of $sp^2$-hybridized carbon atoms arranged in a honeycomb structure, and its characteristics have benefited environmental electrochemistry (Du et al., 2021; Geim and Novoselov, 2007; Huong Le et al., 2019; Le et al., 2015; Mousset et al., 2017, 2016b, 2016a).

The surface morphology of electrode materials is often inspected using microscope devices as a qualitative approach to roughly evaluate the adsorption ability. Microscopic views obtained via scanning electron microscopy (SEM) are displayed in Figs. 3b and 3c for activated carbon fiber (ACF) (Han et al., 2006b) and single-walled carbon nanotube (SWCNT) films (Yue et al., 2019), respectively. Fig. 3b depicts the fine structure of ACF, which involves numerous uniform open pores on the surface (Han et al., 2006b), while the SEM image of the prGO/SWCNT film displays a rough surface and corrugated structures, which should provide a large accessible surface area (Fig. 3c) (Yue et al., 2019).

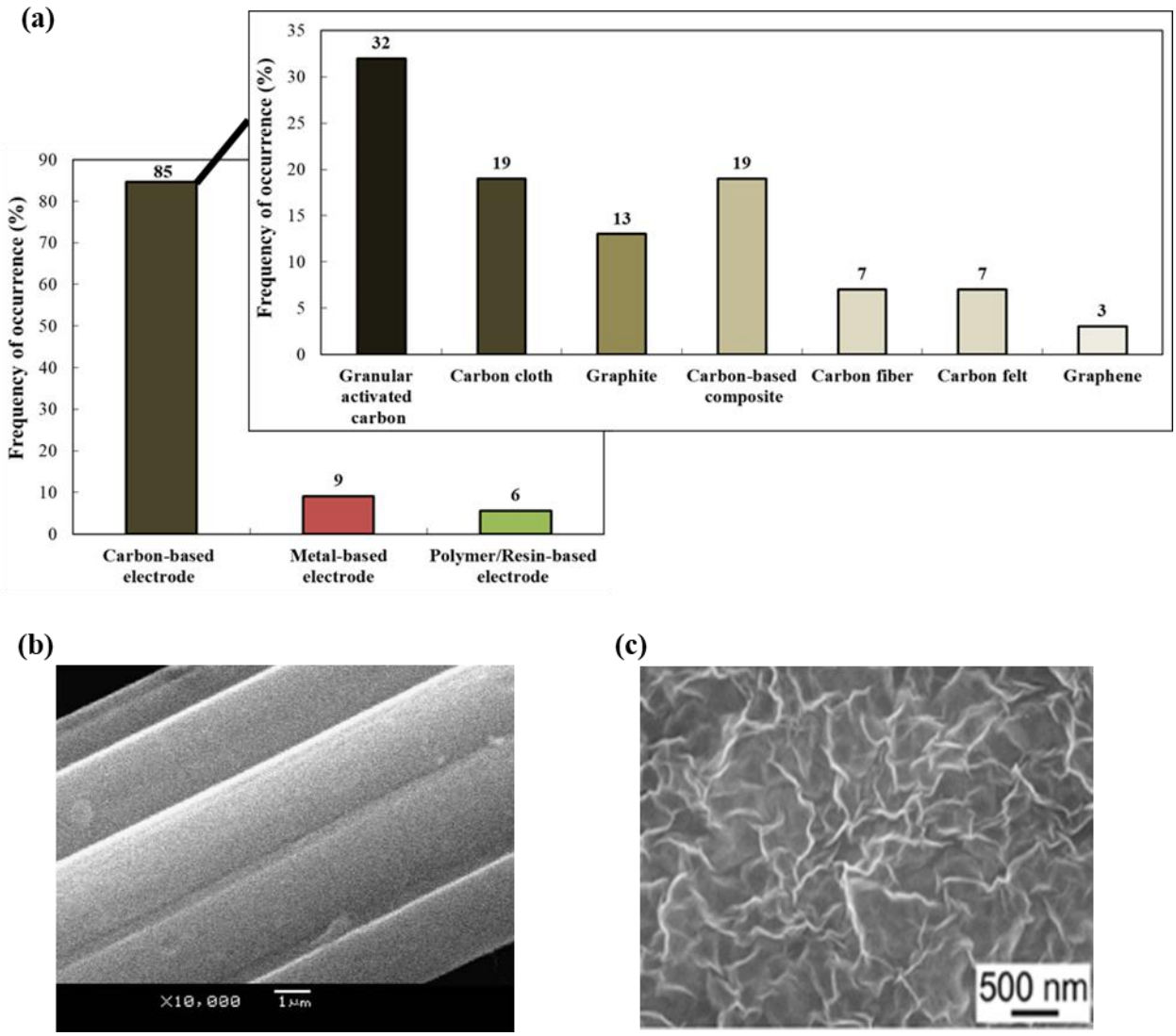


**Fig. 3.** (a) Electrode materials used in the literature, (b) SEM image of ACF (reprinted with permission from (Han et al., 2006b). Copyright 2006, Elsevier), (c) SEM image of the prGO/SWCNT film (Reprinted with permission from (Yue et al., 2019). Copyright 2019, American Chemical Society).

### 3.1.2. Specific surface area, porosity, and roughness

A large surface area and an optimal pore size distribution of the electrode are essential requirements for reaching a high electrosorption capacity. They result in a high capability for charge accumulation at the active sites of the electrode/electrolyte interface (Zaharaddeen et al., 2016). From Fig. 4a, it can be seen that the specific surface area of the electrode used in

the literature reached 2000 $m^2$ $g^{-1}$, while a majority of articles (36%) applied materials with specific surface areas within the range of 0-500 $m^2$ $g^{-1}$ (Table 1).

One of the most common methods employed to modify the surface area and pore size distribution of carbon materials is their activation via chemical and/or thermal treatment. The electrosorption of 4-chlorophenol was studied by testing AC with different treatments, i.e., nonmodified AC (AC-NM), AC oxidation with nitric acid (AC-NA), AC treated with ammonia (AC-Am), and annealed AC (AC-HT) (Fig. 4b) (Biniak et al., 2013). The results highlighted a decrease in the specific surface area ($S_{BET}$) estimated by the well-known Brunauer-Emmett-Teller method when the AC was modified. Additionally, the total volume of mesopores ($V_{me}$) increased with the chemical treatment (AC-NA and AC-Am) (Fig. 4b), while the electrosorption efficiencies were better with these materials. It is important to note that increasing the surface area of materials does not systematically lead to a higher electrosorption efficiency, unlike many studies intend to show. Therefore, the distribution of pores remains an essential factor to consider, along with the specific surface area. The pore size has previously been shown to induce a change in the EDL. Fig. 4c depicts the EDL within different pore sizes of the carbon material, i.e., higher than 2 nm, between 1 and 2 nm and smaller than 1 nm. It has been emphasized that the existence of an optimal pore size gives an optimal capacitance when the pore size is close to the ion size (Largeot et al., 2008). This feature further highlights the impact of microporosity on the EDL and electrosorption efficiency. Due to these differences in the behavior of EDLs in porous materials, a multiscale model has been proposed according to the pore size for a better accuracy of capacitance prediction: sandwich-type model for micropores (< 2 nm), electric double-cylinder model for mesopores (2-50 nm)), and planar model for macropores (> 50 nm) (Fig. 4d) (Dai et al., 2020; Feng et al., 2010; Huang et al., 2008).

A more recent approach for modifying the material properties is to involve carbonaceous nanostructured materials, such as graphene and/or carbon nanotubes (CNTs). A comparison between the specific surface area and porosity of three graphene-based materials, namely, prGO/SWCNTs, prGO and reduced graphene oxide (rGO), used for MB electrosorption has been performed (Yue et al., 2019). The specific surface areas of rGO (5.5 $m^2$ $g^{-1}$) and prGO (29 $m^2$ $g^{-1}$) were much smaller than that of prGO/SWCNT (94 $m^2$ $g^{-1}$), and the same trend was obtained for the total pore volume. Knowing that the prGO/SWCNT electrode material depicted a higher electrosorption capacity (13 g $g^{-1}$), the increase in the specific surface area and total porosity could have explained the higher electrosorption capacity (Yue et al., 2019).

In addition, many electrode materials used in electrosorption can be considered to have a nonidealized electrode geometry, which then affects the EDL and consequently the electrosorption efficiency (Fan et al., 2014). For example, curvature effects are frequently encountered in cylindrical shapes (e.g., CNTs) and porous materials, which breaks with the linearity of models developed for planar electrode systems (Henstridge et al., 2010; Lian et al., 2016). Moreover, differences have been predicted by using density functional theory (DFT) between concave and convex shapes. Concave induces a lower curvature effect than convex interfaces, leading to higher capacitances in the later (Lian et al., 2016), and therefore better electrosorption.

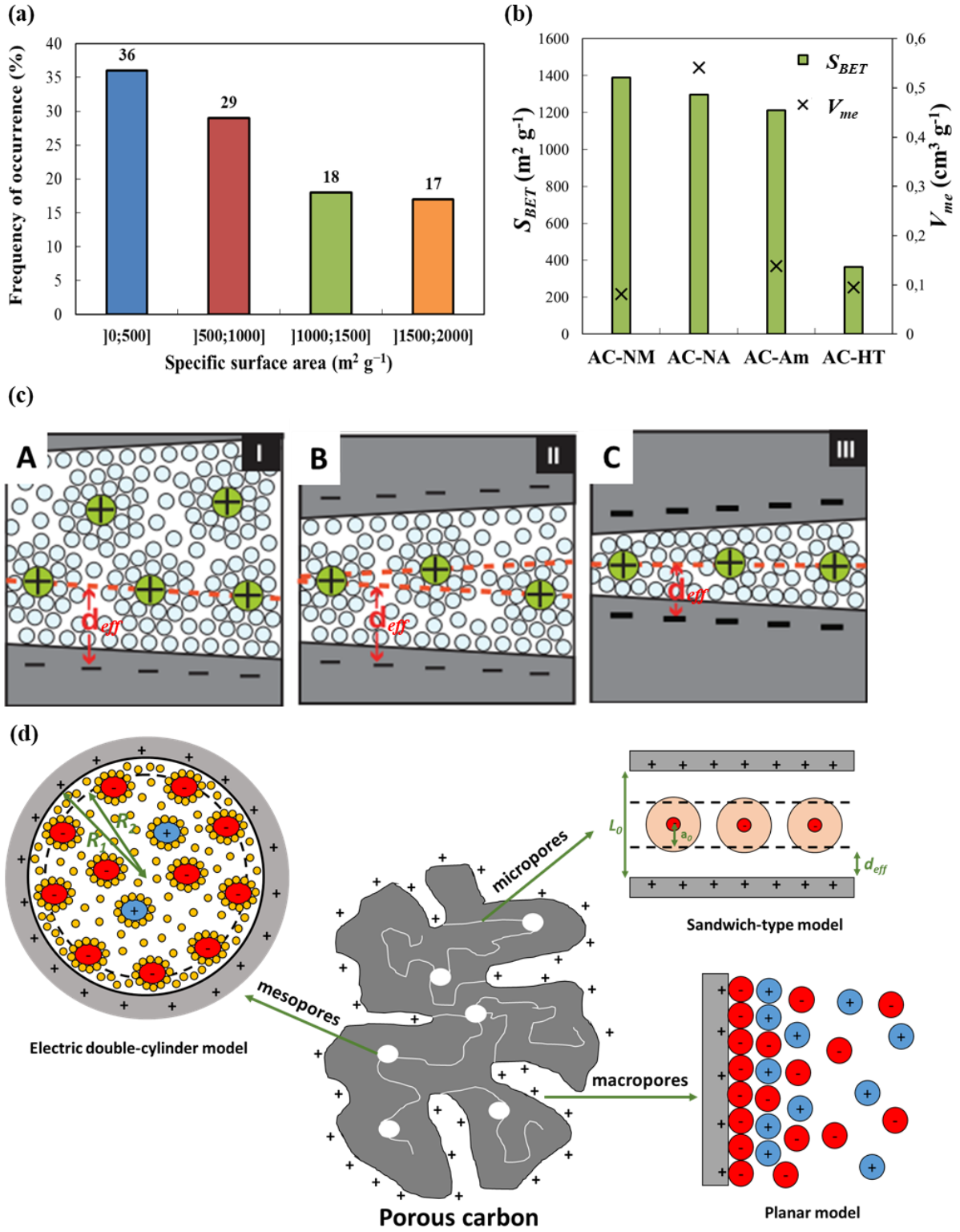


**Fig. 4.** (a) Range of the specific surface area of the electrode implemented for organics electrosorption in literature, (b) $S_{BET}$ and $V_{me}$ evolutions as a function of modified (AC-NA, AC-Am, AC-HT) and AC-NM (Adapted with permission from (Biniak et al., 2013). Copyright 2013, Elsevier), (c) EDL drawings representing solvated ions within different

negatively charged pore sizes in carbon material: higher than 2 nm (A), between 1 and 2 nm (B) and smaller than 1 nm. (Adapted with permission from (Chmiola et al., 2006). Copyright 2006, American Association for the Advancement of Science), (d) Schematic diagrams of a positively charged porous carbon material and the associated model of the EDL: sandwich-type model for micropores, electric double-cylinder model for mesopores, planar model for macropores (Adapted with permission from (Huang et al., 2008) (Copyright 2008, Wiley), (Feng et al., 2010) (Copyright 2010, American Chemical Society), (Dai et al., 2020) (Copyright 2020, American Chemical Society)).

### 3.1.3. Material conductivity

It is well known that the electrical conductivity of electrode materials increases the rate of electron transfer at the material/electrolyte interface (Du et al., 2021). The effect of electrical conductivity on the electrosorption efficiency has been particularly emphasized. It has been shown that the higher electrosorption capacity obtained with prGO/SWCNTs compared to prGO and rGO was partly related to the electrical conductivity of prGO/SWCNTs (74 S $cm^{-1}$), which was far larger than that of prGO (20 S $cm^{-1}$) and rGO (30 S $cm^{-1}$) (Fig. 5a) (Yue et al., 2019). The electrical conductivity increased with the introduction of SWCNTs in the samples. Other authors have also reported the positive effect of increasing the electrical conductivity on the kinetics and capacity of electrosorption (Alencherry et al., 2017).

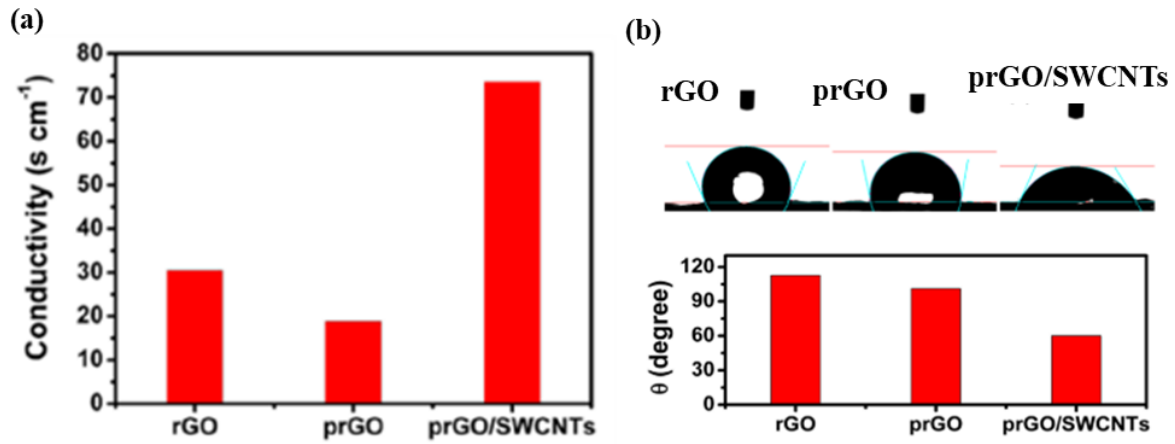


**Fig. 5.** (a) Electrical conductivity of rGO, prGO and prGO/SWCNT materials (reprinted with permission from (Yue et al., 2019). Copyright 2019, American Chemical Society), (b) Surface wettability of rGO, prGO and prGO/SWCNT materials (adapted with permission from (Yue et al., 2019). Copyright 2019, American Chemical Society).

### 3.1.4. Surface functions

The type of surface function on the porous electrode can affect the electrosorption process. A comparison of electrosorption efficiencies using AC with different surface functions (Biniak et al., 2013) has been reported. AC-Am produced basic nitrogen-containing functional groups on the surface, while AC-NA increased the number of acidic oxygen functional groups bound to the surface. The more acidic the carbon surface, the more oxygen that was bound to it and the lower the efficiency of 4-chlorophenol electrosorption (Biniak et al., 2013). In another study, the incorporation of spherical polystyrene and SWCNTs into graphene oxide (prGO/SWCNTs) led to a higher electrosorption capacity than that of rGO and porous rGO films (Yue et al., 2019). Spherical polystyrene generated 3D macropores, while SWCNTs created efficient pathways for the transfer of ions and electrons.

### 3.1.5. Surface wettability

The surface wettability of the electrode is a parameter that can be obtained by measuring the contact angle. If the contact angle is greater than 90°, the electrode is hydrophobic, while if it is less than 90°, the electrode is considered hydrophilic (Yue et al., 2019). This factor has barely been quantified in electrosorption studies, although it has been established that a poor wettability generally hampers ion (hydrophilic) transport within the pores of the electrode. This is unfavorable for the electrosorption process (Chang et al., 2014). Nevertheless, a recent study stated the influence of the wettability of three graphene-based materials (prGO/SWCNTs, rGO and prGO) on MB electrosorption (Yue et al., 2019). The surface wettabilities were 60°, 113° and 101° for prGO/SWCNTs, rGO and prGO, respectively (Fig. 5b) (Yue et al., 2019). The prGO/SWCNTs showed a higher hydrophilicity, and the electrosorption capacity (up to 13 g $g^{-1}$) was higher than that of the two other materials. The introduction of SWCNTs improved the hydrophilicity of the prGO/SWCNTs. Therefore, the surface wettability also influences the electrosorption capacity of organic compounds, and should not be neglected in investigation studies.

## 3. 2. Applied electrode potential/current density and electrode polarity

The electrode polarity related to the applied current intensity sign is known to influence the electrosorption capacity of the porous surface, while the electrosorption rate can be increased. According to the reviewed papers (Table 1), the occurrence percentages of electrode polarity configurations tested for electrosorption are as follows: cathode (23%), anode (41%) and both polarities (i.e., cathode and anode) (36%) (Fig. 6a). Most of the time, the electrode polarity can induce electromigration effects that need to be considered according to the charge in the targeted compounds. Since many organic compounds are negatively charged, the reason why more electrosorption studies have been performed with a positively charged anode material

could be explained (Fig. 6a). For instance, the electrode polarity was studied by using metal wire coated with an epoxy resin-based polymer as the working electrode and platinum wire as the counter electrode for cresol red electrosorption (Wang et al., 2012). The results showed that anodic polarization enhanced the efficiency compared to cathodic polarization. This was explained by the orderly migration of the negatively charged cresol red molecules with the sulfonic group on the benzene ring toward the positively charged wire anode. In contrast, the same charge between the compound and the cathode material limited their interaction (Wang et al., 2012). In a similar way, anodic polarization increased the amount of phenol adsorbed on AC, while cathodic polarization decreased it (McGuire et al., 1985). In contrast, the cathodic polarization remarkably increased the thiocyanate anion electrosorption on the AC compared to anodic polarization (Rong and Xien, 2005), which was ascribed to coulombic interactions. In addition, the cathodic electrosorption of 8-quinolinecarboxylic acid on ACC resulted in higher removal efficiencies (96%) than anodic electrosorption (84%) (López-Bernabeu et al., 2016). These differences in behavior were due to the occurrence of a faradaic reaction at the Ti-Pt anode, while cloth was the cathode. In this configuration, the anodic oxidation of 8-quinolinecarboxylic acid and its subsequent byproducts could be implemented, which enhanced the removal efficiency of the targeted compound (López-Bernabeu et al., 2016). In contrast, there was no oxidation of organic compounds when the AC tissue was used as the anode, and only electrosorption could occur.

The faradaic reactions are considered to be competitive when only electrosorption is desired. Their occurrence is directly related to the applied electrode potential value, which is the driving force that permits modification of the adsorption equilibrium by introducing a difference in the potential at the electrode/electrolyte interface. This potential is linked with the applied current density through the Butler-Volmer equation (Lord et al., 2012). These reactions are involved at either anodic potentials that are too high or cathodic potentials that are too low, and some of them have recently been reviewed (Zhang et al., 2018b) and

schematized (Holubowitch et al., 2017). Water oxidation into oxygen ($O_2$) and water reduction into hydrogen ($H_2$) are the two most famous faradaic equations that can occur in aqueous media. There can be other parasitic reactions according to the electrode material used and/or the composition of the electrolyte. For instance, if a carbon material is used as an anode, it can be easily oxidized ($E^0$ = 0.21 V/standard hydrogen electrode). This can be an issue because most of the porous electrodes employed are based on a carbon material (Fig. 3a), knowing that anodic polarization is the most experimented upon (Fig. 6a). Therefore, caution should be taken in applied operating conditions if porous carbon anodes are implemented to avoid corrosion. Moreover, undesirable nitrogenous and/or chlorinated oxyanions ($NO_2^-$, $NO_3^-$, ClOH, $ClO_3^-$) can be initially generated at a sufficiently high anodic potential in the presence of nitrogenous species and/or chloride ions (Brito et al., 2015; Mousset et al., 2020, 2018b). When a high $O_2$ overvoltage anode is employed, such as boron-doped diamond (BDD), to cite the most frequently studied anode, perchlorate ($ClO_4^-$) can even be produced (Bergmann et al., 2009). Often missing in the literature and especially in reviews dealing with faradaic reactions involved in capacitive deionization (Zhang et al., 2018b): the local alkalization at the cathode from $O_2$ reduction and $H_2O$ reduction reactions should not be overlooked. Under this condition, magnesium, calcium and/or carbonate are present in solution, which is the case in many actual aqueous effluents (Adnan et al., 2021a; Belarbi et al., 2016), and electroprecipitation phenomena can occur by forming $Mg(OH)_2$ and/or $CaCO_3$ at the cathode surface (Adnan et al., 2021a; Belarbi et al., 2016). These deposits then progressively passivate the cathode and hamper electrolysis.

Thus, faradaic reactions can be avoided if a sufficiently short potential window is applied, whose range can be verified by a voltammetric analysis. This is a further advantage in terms of the energy consumption because the cell potential remains low. In this capacitive voltage range, it has been shown that an increase in the applied potential from open circuit (OC) to 600 mV involved increases in the rate and capacity of AO7 electrosorption into ACF (OC:

1.12 mmol $g^{-1}$, 200 mV: 1.17 mmol $g^{-1}$, 400 mV: 1.39 mmol $g^{-1}$, and 600 mV: 1.84 mmol $g^{-1}$)) (Fig. 6b) (Han et al., 2008). Similarly, an intensification of polarization caused an increase in the percentage of BA electrosorption onto ACC (OC: 52%, -200 mV: 50%, -600 mV: 44%, -900 mV: 15%, +200 mV: 72%, +600 mV: 75%, +900 mV: 74%). This was explained by an amplification of the electrostatic interaction between the ACC surface (positively charged) and benzoate anion (negatively charged) with rising potentials (Bayram and Ayranci, 2012b).

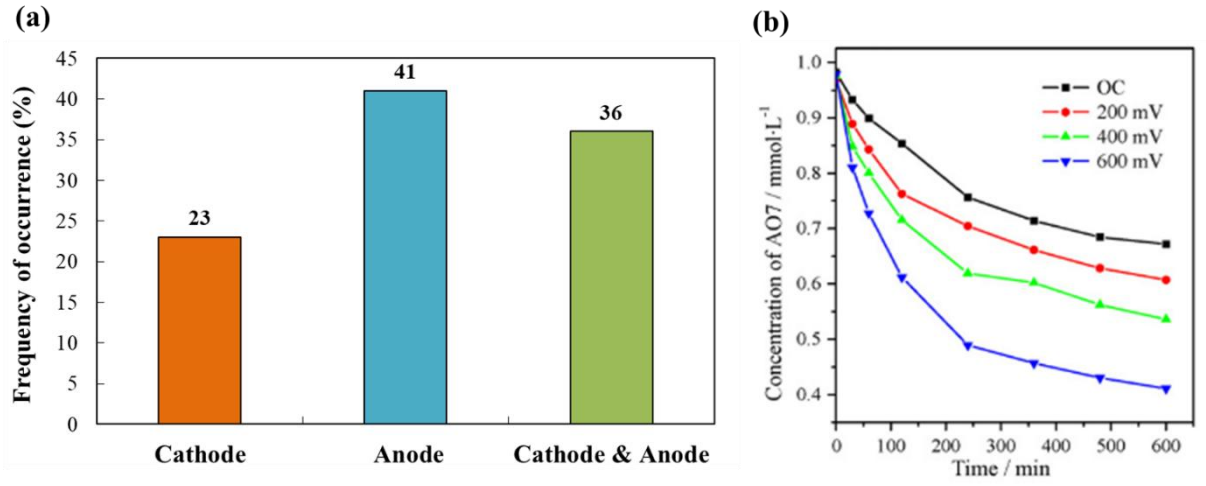


**Fig. 6.** (a) Occurrence percentages of electrode polarity configurations tested for electrosorption in the literature, (b) effect of the working electrode potential on AO7 electrosorption (Reprinted with permission from (Han et al., 2008). Copyright 2008, Elsevier).

## 3. 3. Physico-chemistry of the electrolyte solutions

### 3.3.1. Type and concentration of the inorganic electrolyte

In most synthetic solution studies, an inorganic supporting electrolyte is added to increase the electrical conductivity of the wastewater to be treated (Gerçel, 2016; Han et al., 2006b; Koparal et al., 2002). Although electrolytes should not be added in the context of wastewater depollution to avoid external contamination, studies in their presence have emphasized the antagonist role of the electrosorption efficiency in organics according to their types and concentrations.

It has been highlighted that the equilibrium electrosorption capacity of phenol on ACF was reduced, whereas the electrosorption rate was enhanced with an increasing sodium sulfate ($Na_2SO_4$) electrolyte concentration from 1 to 100 mM (Han et al., 2006b). $Na_2SO_4$ increased the solution conductivity, which contributed to an increase in the ion transport. However, the adsorption sites for phenol on the surface of the adsorbent were occupied by the competitive electrosorption of the $Na_2SO_4$ electrolyte (Han et al., 2006b). Similar results have been obtained in other studies involving the electrosorption of aniline on ACF in $Na_2SO_4$ electrolyte (Fig. 7a) (Han et al., 2006a), of 2,4-dichlorofenoxyacetic acid on ACC in $Na_2SO_4$ electrolyte (Bayram et al., 2018), and of acilan blau dye on AC-perlite mixtures in sodium chloride (NaCl) electrolyte (Han et al., 2006b). This trend was confirmed by the study of 1-adamantanol in the presence of halide ($F^-$, $Cl^-$, $Br^-$)-based electrolytes. This further emphasized the decrease in the organic adsorption when the electrolyte concentrations increased from 5 to 100 mM, regardless of the types of halide anions (Stenina et al., 2001). It was thus reported that organic-inorganic attraction could occur during concurrent adsorption, which could be explained by the strong hydrogen bonds between the $OH^-$ group of the organic compound and the halide anions.

The effect of the electrolyte type on the electrosorption efficiency was more emphasized by Gerçel (2016), who compared two different electrolytes, either sodium nitrate ($NaNO_3$) or $Na_2SO_4$, for the electrosorption of burdem orange II textile dye by using AC prepared from a waste material. The highest dye removals of 95% and 88% was achieved with 0.2 M $Na_2SO_4$ and 0.2 M $NaNO_3$, respectively. The differences in removal percentages could be attributed to the different hydrated radii and valences of the electrolyte, regardless of the initial solution concentration (Gerçel, 2016).

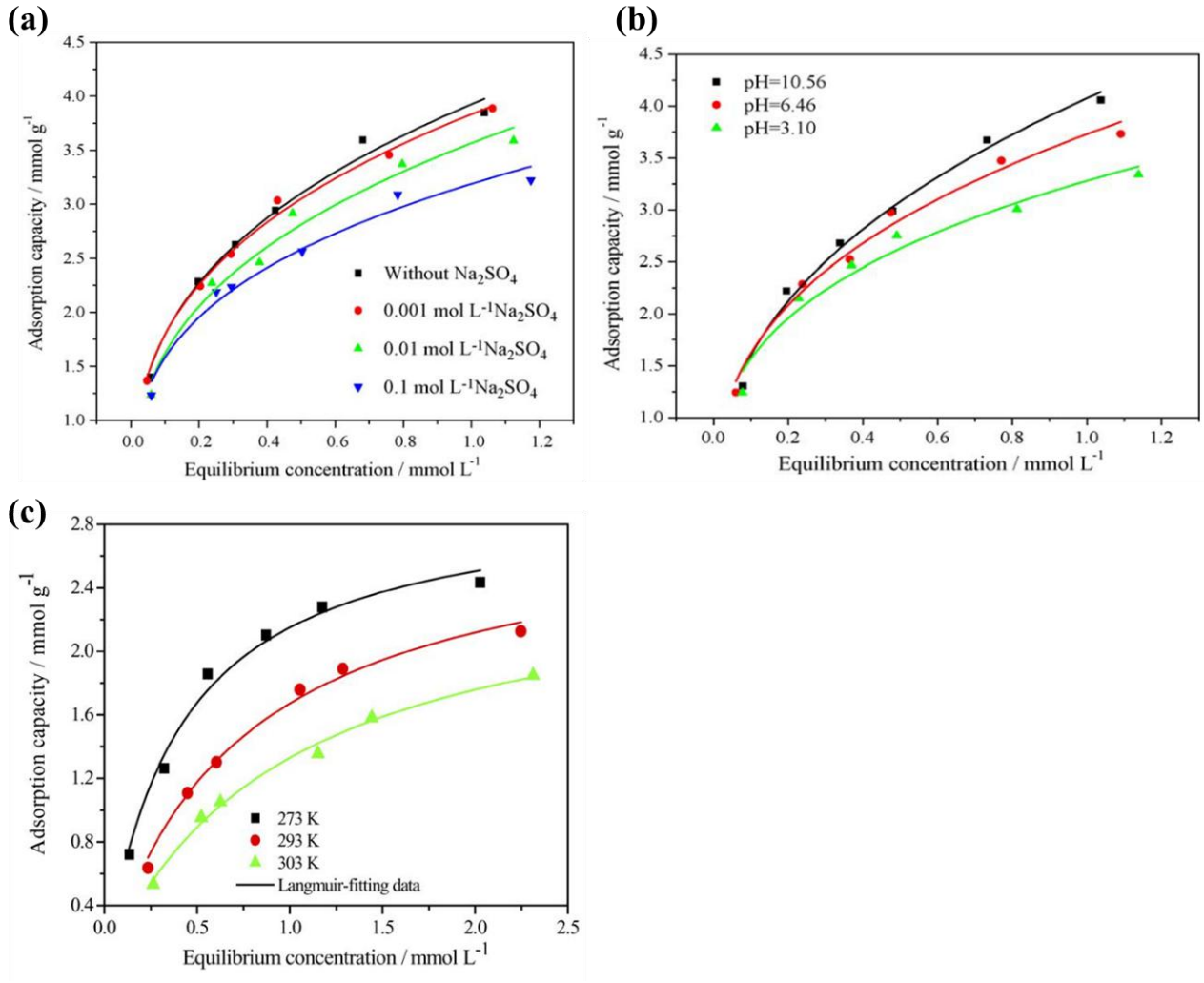


**Fig. 7.** Effect of (a) the initial concentration of the electrolyte on aniline electrosorption in the $Na_2SO_4$ electrolyte (a) (Reprinted with permission from (Han et al., 2006a). Copyright 2006, Elsevier), (b) pH on the aniline electrosorption (Reprinted with permission from (Han et al.,

519 2006a). Copyright 2006, Elsevier), (c) temperature on the phenol electrosorption (Reprinted
520 with permission from (Han et al., 2006b). Copyright 2006, Elsevier).

521

522 **3.3.2. pH**

523 The initial pH of the electrolyte solution is an important factor, since it can influence the
524 ionization state of the outer electrode surface and the surface electrical charge characteristics
525 of pollutants, as well as the electrosorption mechanism. Therefore, it also influences the
526 electrosorption capacity of the organic compounds.

527 Table 3 summarizes the optimum pH for a variety of organic pollutants whose acid
528 dissociation constants (pKa) have been reported. The effect of pH within the range of 4 to 12
529 on the electrosorption capacity of cresol red using electrodes made of stainless steel wire
530 coated with a nonconductive polymer was studied (Wang et al., 2012). Compound
531 electrosorption was optimal at pH 6.0 due to the respective protonation and deprotonation of
532 cresol red in acidic and basic media considering its pKa values of 0.5 ($pKa_1$) and 8.5 ($pKa_2$).
533 Protonation in a strong acid medium would lead to the molecular ionization of cresol red,
534 which explains the weak electrosorption in acidic media. Conversely, deprotonation would
535 lead to the electrosorption of cresol red anions. The influence of the initial pH values covering
536 a range from 3.1 to 10.6 on aniline (pKa = 4.6) electrosorption on ACF was also investigated
537 (Han et al., 2006a). The electrosorption capacity of aniline rose with an increasing pH as
538 shown in Fig. 7b. This was attributed to the electrostatic interaction caused by protonation or
539 deprotonation according to the pH changes, but could also be due to the electron donor ability
540 of the amino group that increased in a basic solution. Similar results have been obtained in
541 other studies regarding the electrosorption of aniline (Chai et al., 2007) and mercury (II)
542 acetate (Jayson et al., 1987).

In contrast, the electrosorption capacity decreased with an increasing pH from 4 to 12 when bentazone (pKa = 3.3) was removed from aqueous solutions using an ACC electrode (Ania and Béguin, 2007). This trend was due to the pH dependence of the charges on the carbon cloth surface and of the bentazone ionization. At an acidic pH, the bentazone is mainly nondissociated, and all acidic groups are protonated (neutralization of the negative charges), which minimizes the repulsive electrostatic interactions, and the electrosorption is improved. At a higher pH, the anionic form predominates in the solution, which implies a weaker interaction of the carbon cloth surface with deprotonated bentazone than with its neutral form. Similarly, the electrosorption of BA was lower at a basic pH than at an acidic pH, which was ascribed to the competition between the benzoate (formed at basic pH) and $OH^-$ anions for the positively charged ACC anode material (Bayram and Ayranci, 2012a). A similar trend was obtained with the electrosorption of thiocyanate (pKa = 0.5) (Rong and Xien, 2009, 2005), benzene (pKa = 43) (Heiland et al., 1966), naphthalenesulfonic acid (pKa = 0.2), benzyl alcohol (pKa = 15.4), naphthoic acid (pKa = 4.2), methylquinolinium chloride (Bán et al., 1998) and burdem orange II (pKa = 11.4) (Gerçel, 2016) (Table 2).

**Table 2.** Optimal initial solution pH during the electrosorption of selected pollutants.

| Pollutant | pH range | Optimum pH | pKa | Reference |
|---|---|---|---|---|
| Cresol red | 4.0 – 12.0 | 6.0 | $pKa_1 = 0.5$; $pKa_2 = 8.5$ | (Wang et al., 2012) |
| Bentazone | 2.0 – 7.0 | 2.0 | 3.3 | (Ania and Béguin, 2007) |
| Aniline | 3.1 – 10.6 | 10.6 | 4.6 | (Han et al., 2006a) |
| Thiocyanate | 0 – 11.0 | 3.0 | 0.5 | (Rong and Xien, 2005) |

| | | | | |
|---|---|---|---|---|
| Burden orange II | 2.0 – 6.5 | 2.0 | 11.4 | (Gerçel, 2016) |
| BA | | 4.28 | 4.2 | |
| Phthalic acid | 2.93 – 10.54 | 3.98 | $pKa_1 = 2.92$; $pKa_2 = 5.41$ | (Bayram and Ayranci, 2012a) |
| NA | | 3.62 | $pKa_1 = 2.05$; $pKa_2 = 5.81$ | |
| Benzene | 0.5 – 11.0 | 0.5 | 43 | (Heiland et al., 1966) |

560

561 **3.3.3. Temperature**

562 Generally, the temperature affects the electrosorption capacity. Many different enthalpies of
563 adsorption ($\Delta H_{ads}$) values have been presented in the literature that attest to the variabilities
564 of thermodynamic processes and the influence of temperature. Ethylene electrosorption on
565 platinum was studied at temperatures varying from 303 to 343 K (Gileadi et al., 1965). The
566 equilibrium adsorption constant was essentially independent of the temperature; consequently,
567 $\Delta H_{ads}$ equaled 0. In contrast, the electrosorption of phenol on ACF at three temperatures, 273,
568 293, and 303 K, was temperature-dependent (Fig. 7c) (Han et al., 2006b). The electrosorption
569 process was more favorable at lower temperatures, and $\Delta H_{ads}$ was negative, which showed
570 that phenol was exothermally adsorbed by ACF. This further highlights that electrostatic
571 interactions and dipole–dipole interactions might be the main adsorption mechanism for
572 phenol electrosorption on ACF (Han et al., 2006b). The temperature also affected aniline
573 electrosorption on the ACF electrode at temperatures varying from 293 to 343 K (Chai et al.,
574 2007). The electrosorption efficiency increased with an increasing temperature until reaching
575 a peak at 313 K and then gradually decreased. This was due to the increase in the diffusion
576 rate of aniline through the static aqueous layer at the fiber/solution interface. At temperatures
577 higher than the optimal value, the efficiency did not increase, since aniline electrosorption
578 was an exothermic process (Chai et al., 2007). Another study varied the temperature of the

electrolyte from 283 to 323 K for butanol and 1-oxyadamantane electrosorption (Stenina et al., 2009). An increase in the temperature led to an increase in the capacitance from 4.9 to 5.5 μF $cm^{-2}$, and therefore in the electrosorption efficiency (Stenina et al., 2009). Thus, the increase in the temperature either decreased or increased the electrosorption capacity, according to the natures of the pollutants and of the active sites on the electrodes.

## 3. 4. Types of organic pollutants, their co-sorption, and the initial concentration effects

According to the papers reviewed, 92% of the electrosorption studies focused on aromatic compounds, while only 8% focused on aliphatic pollutants (Fig. 8a). Surprisingly, 100% of articles dealt with artificial contamination. This highlights the crucial need to deal with actual wastewater to consider other matrix effects in the electrosorption efficiency, such as competition with co-sorption, clogging, etc.

In real matrices, the presence of multiple compounds is unavoidable; therefore, co-sorption studies remain essential. Several articles focused on these aspects, but in simulated wastewater. The co-sorption effect in the presence of three organic pollutants (acid red 88, orange II, and MB) on a three-dimensional (3D) graphene aerogel electrode was studied (Sun et al., 2016). The electrosorption rate of the dyes ranked as follows (with an increasing rate): acid red 88 < orange II < MB (Fig. 8b). This was inversely correlated with the size of the dye molecules (with an increasing size): MB < orange II < acid red 88. Thus, smaller molecules would find more pores accessible for electrosorption. The influence of the charge of the dyes must also be considered, because it affects the electrostatic force between the adsorbent and the molecules and controls the electrosorption process. For instance, π–π interactions have been shown to play an important role, since dyes with more aromatic rings showed stronger

603 interactions with the adsorbent (Sun et al., 2016). In addition, the charge dipole and dispersion
604 interactions between the adsorbent and the aromatic organic acids have also depicted an
605 influence on the electrosorption. The electrosorptive behavior of aromatic organic acids (i.e.,
606 benzoic, phthalic and NA) onto the ACC electrode was further examined (Bayram and
607 Ayranci, 2012a). The rate constants of electrosorption of the acids decreased in the following
608 order: NA > phthalic acid > BA (Bayram and Ayranci, 2012a). A more recent study
609 schematized the material/solution interface in the presence of MB sorption on a
610 prGO/SWCNT surface (Fig. 8c) (Yue et al., 2019). In the absence of an electric current, i.e.,
611 under OC conditions, the dye randomly adsorbed on the material, leading to a lower
612 adsorption capacity. In contrast, the positively charged pollutant could adsorb onto the
613 negatively charged material under cathodic polarization, which enhanced the sorption
614 efficiency. The importance of the electrode potential and intermolecular interaction was also
615 emphasized in co-electrosorption studies from Damaskin's group (Damaskin, 2011, 2009,
616 2008; Damaskin et al., 2003; Damaskin and Baturina, 2001a, 2001b, 2001c, 1999; Stenina et
617 al., 2001). Furthermore, all these trends corroborated the behavior at the electrode/electrolyte
618 interface. The characteristics of anions and cations (e.g., radii, interactions with solvent,
619 charge, etc.) of the electrolyte have been identified as the key role parameters for controlling
620 the distribution and concentrations of ions in EDL, and therefore greatly impact the
621 electrosorption efficiency (Kornyshev, 2007; Waegele et al., 2019).

622

623 The influence of the initial concentration of organic compounds on the electrosorption
624 efficiency has been widely reported in the literature, especially in batch mode configurations.
625 The electrosorption efficiency was studied by varying the initial MB concentration from 10 to
626 600 mg $L^{-1}$ (Yue et al., 2019). The increase in the pollutant concentration up to 100 mg $L^{-1}$
627 led to an increase in the electrosorption capacity at a given time, and thereafter remained

constant at higher initial concentrations. Similarly, a kinetics study observed an increase in the rate of metribuzin electrosorption on GAC with an increase in the initial concentration from 0.23 to 2.1 mmol $L^{-1}$, leading to a higher capacity at identical times (Kitous et al., 2009). Similar trends have been obtained with the electrosorption of acilan blau dye (Koparal et al., 2002), phenol (Han et al., 2006b), ethylene (Gileadi et al., 1965), AO7 (Han et al., 2008), β-naphthol (Eisinger and Alkire, 1980), AO8, AY14, AR151 (Sahin et al., 2020), bentazone (Ania and Béguin, 2007), naphthalenesulfonic acid, benzyl alcohol, naphthoic acid, methylquinolinium chloride (Bán et al., 1998) and MB (Fig. 8d) (Nainamalai et al., 2018). These studies were performed in batch mode, meaning that not only the kinetics of electrosorption were quicker, but also the capacities were higher with an increasing initial concentration. This is formally disclosed with isotherm models discussed in section 4.1. This trend might be explained by the decrease in the driving force of the concentration gradient of pollutants toward the surface of the working electrode during an increase in loading rate (Han et al., 2006b). Moreover, the affinity between the pollutant and the electrode surface was significantly increased by polarization, allowing the enhanced adsorption capacity of pollutants on the electrode (Yue et al., 2019). Furthermore, different EDL behaviors at high concentrations of organic electrolytes have been highlighted, since conventional concepts of EDLs, such as the Gouy-Chapman-Stern representation, remain suitable only for diluted media. In dense mixtures, nonlinear polarization at the interface has been noticed, while a capacitance-voltage dependence was emphasized (Bazant et al., 2011). At a low voltage, a so-called overscreening model is assumed, which is formed by a monolayer of ions and an excess of counterions in the second monolayer (Fig. 8e) (Bazant et al., 2011). In contrast, at a medium voltage, there is a condensed layer formation of counterions, and at even higher voltages, complete lattice saturation is expected (i.e., the formation of two monolayers at the interface), which is defined as the crowding model (Fig. 8e) (Bazant et al., 2011).

From a practical point of view, the continuous mode is preferred, and the variation in the initial concentration will mainly affect the kinetics of electrosorption, while the maximum capacity of the adsorbent can be reached by adapting the contact time. The reactor volume and/or the adsorbent quantity can also be adjusted to reach the maximum electrosorption efficiency, as discussed in section 3.5.

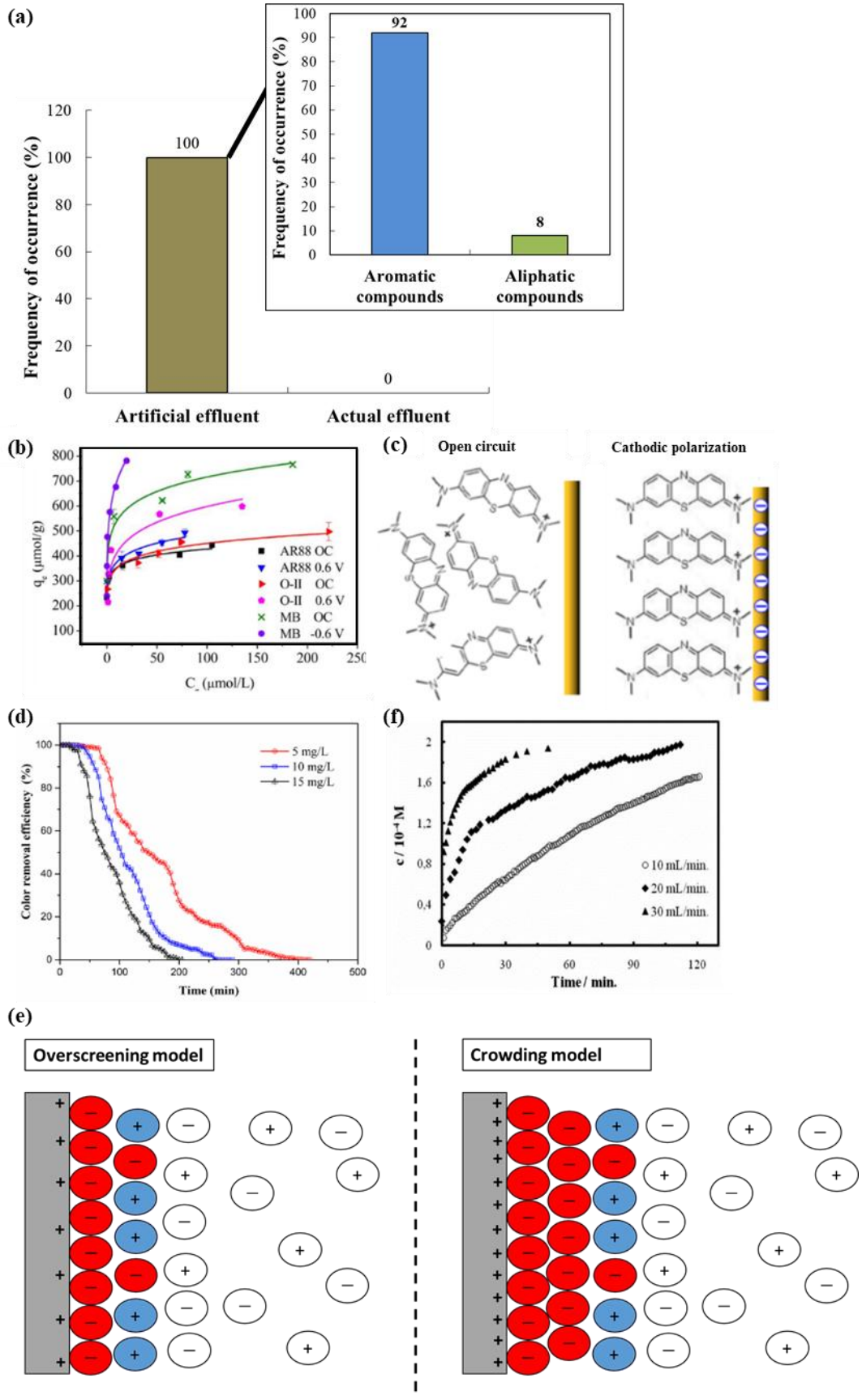


659

660 **Fig. 8.** (a) Type of effluent studied in the literature, i.e., artificial or real contamination and

661 the presence of either aromatic or aliphatic compounds during electrosorption processes, (b)

effect of acid red 88, orange II, and MB co-sorption (Reprinted with permission from (Sun et al., 2016). Copyright 2016, American Institute of Chemical Engineers Journals), (c) schematic representation of MB molecule orientation on the prGO/SWCNT surface (Reprinted with permission from (Yue et al., 2019). Copyright 2019, American Chemical Society), (d) influence of the initial concentration on MB electrosorption (Reprinted with permission from (Nainamalai et al., 2018). Copyright 2018, Elsevier), (e) overscreening versus crowding models of EDL in the presence of concentrated electrolyte (e.g., ionic liquids) (Adapted with permission from (Bazant et al., 2011). Copyright 2011, American Physical Society), (f) impact of the flow rate on 2,4-dichlorophenoxyacetic acid electrosorption (Reprinted with permission from (Bayram et al., 2018). Copyright 2018, IWA Publishing).

## 3. 5. Residence time, flow rate, reactor volume, and adsorbent load

The electrosorption efficiency is also controlled by the residence time and volume flow rate, which are both related to the reactor volume. All previous works reported an enhancement in the electrosorption capacity with an increasing residence time and a decreasing flow rate by maintaining the contact of the pollutants with the active sites of the porous electrode. For example, a decrease in the MB electrosorption onto AC was reported with increased flow rates from 3 to 9 mL $min^{-1}$ (Nainamalai et al., 2018). Similar trends have been observed with 2,4-dichlorophenoxyacetic acid (Fig. 8f) (Bayram et al., 2018), acilan blau dye (Koparal et al., 2002), burdem orange II (Gerçel, 2016), BA and NA (Bayram, 2016), metribuzin (Kitous et al., 2009) and BA (Bayram and Ayranci, 2012b) electrosorptions. It was assumed that the EDL thickness at the polarized adsorbent surface decreased with an increasing flow regime (Bayram et al., 2018). Consequently, the specific double layer capacitance ($C_{dl}$) value was reduced along with the electrosorption capacity.

686 The adsorbent load is another way to increase the electrosorption capacity. The influence of
687 the bed heights, and therefore the adsorbent load, on MB electrosorption was studied
688 (Nainamalai et al., 2018). When the bed height increased from 3 to 9 cm, the MB
689 electrosorption capacity increased from 54 mg $g^{-1}$ to 81 mg $g^{-1}$ caused by an increase in the
690 residence time and the accessible binding sites. Similar trends have been obtained with the
691 electrosorption of β-naphthol (Eisinger, 1983) and acilan blau dye (Koparal et al., 2002).

692

693 ## 3. 6. Reactor design

694 An ideal reactor design for electrosorption needs to meet the requirements to make full use of
695 the electrode surface area while minimizing the mass transfer limitations and maintaining a
696 homogeneous potential distribution. The typical reactor designs developed in general applied
697 electrochemistry have been tested for electrosorption (Table 1). They include systems with
698 fixed-bed or fluidized beds, flow-by or flow-through parallel plate cells and stirred tank
699 reactors (STRs). According to the reviewed papers (Table 1), fixed-bed reactors have been
700 more implemented for organic electrosorption (43%), followed by the flow-through parallel-
701 plate cell design (21%) (Fig. 9). This could be attributed to their adapted design when porous
702 electrode materials are employed. This then enhances the efficiency by benefitting from the
703 internal surface area.

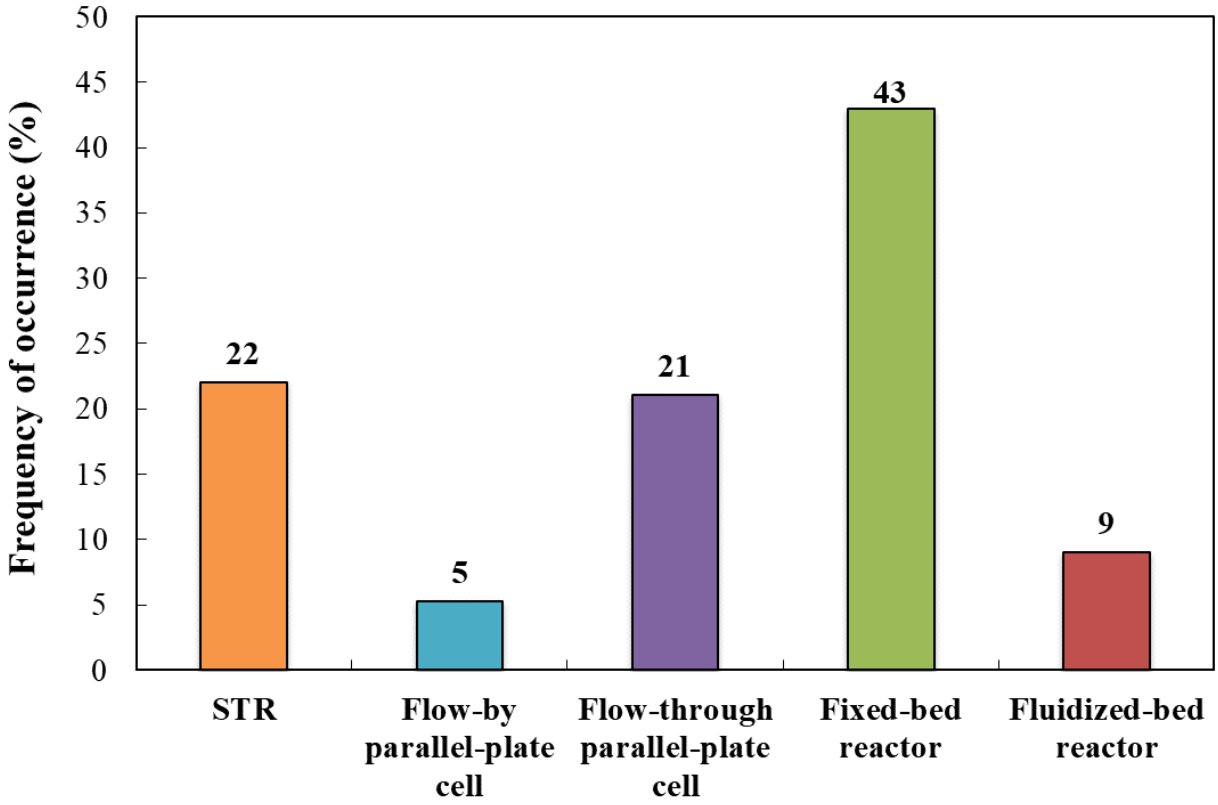


704

705 **Fig. 9.** Occurrence frequency of different electrosorption reactor designs found in the
706 literature.

707

708 The reactor design description and their comparison are described as follows, while Table 3
709 summarizes the advantages and drawbacks of each type of reactor design. Further detailed
710 information regarding the electrochemical reactor design performance for general applications
711 can be found in prominent textbooks in the field (Coeuret and Storck, 1984; Goodridge and
712 Wright, 1983a; Newman, 1968; Pletcher and Walsh, 1982).

713 In STR, the electrode materials are placed in parallel, and the solution is magnetically (lab-
714 scale) or mechanically (pilot-scale) stirred in a tank (Fig. 10a) (Monteil et al., 2019; Mousset
715 and Dionysiou, 2020). The STR configuration was implemented most of the time in batch
716 mode, as opposed to continuous mode. The STR can be useful for laboratory batch studies,

especially for troubleshooting or development works. However, the mass transfer is the worst in these systems. This also leads to a higher footprint area due to the higher required total surface area of the electrode. Consequently, an alternative reactor design is preferred for commercial use.

Conventional flow-by and flow-through parallel plate cells have typically been proposed (Figs. 10b and 10c). Two configurations are possible concerning the direction of the effluent flow with respect to the direction of the current flow. In the flow-by cell, the current and flow of the effluent are perpendicular (Adnan et al., 2021b). The effluent circulates between the electrodes, with a variant with a "channel", which is similar to a flow-by cell in series, i.e., a succession of cathode and anode materials (Mousset and Dionysiou, 2020). In the flow-through cell, the current and flow of the effluent are parallel, and the effluent flows through the porous electrode. This electrode is considered to be thin, which does not constitute beads or particles, and differentiates the flow-through cell from a "bed reactor". An advantage of parallel-plate cells is that they can be implemented in stacks of cells arranged in series and/or in parallel in order to enhance the conversion yield and/or the treatment capacity, respectively. This is adapted for applications at an industrial scale (Kakhi, 2009; Langlois and Coeuret, 1990). The flow-through cell has a distribution of potentials that tends to be less homogeneous than in the flow-by cell. However, the flow-by cell induces mass transfer limitations compared to the flow-through cell, and has therefore been less implemented for electrosorption purposes (Fig. 9). Another possibility with parallel-plate design is the variation in the inter-electrodes distances that decreases the cell resistance and increases the mass transfer at a shortened gap, in addition to affecting the EDL behavior. In more conventional cells, i.e., at millimetric distances, it is considered that an excess charge can occur only at the surface of the material according to Gauss theory. In nanofluidic thin film cells, i.e., at nanometric gaps, the assumption of electroneutrality in the double layer may be

inappropriate. This is because the OHP in EDL theory becomes highly dynamic due to very high mass transport rates of redox ions (Fan et al., 2014).

In parallel, fixed- and fluidized-bed reactors have been suggested as substitute designs. These consist of the effluent circulating through a bed constituted by a volume electrode, i.e., a 3D porous polarized material (Figs. 10d-10g). In the fixed-bed reactor, the electrode particles are all in permanent contact, which defines a monopolar connection mode. In this case, the particulate electrodes constitute a single electron conducting particle that is either completely positively (anode) or negatively (cathode) charged (Goodridge and Wright, 1983b). In the fluidized-bed reactor, the electrode particles are not in contact with each other, which leads to a bipolar mode (López-Bernabeu et al., 2016). This means that one side of each particle is positively charged, while the other side of the particle is negatively charged (Goodridge and Wright, 1983a). Most of the time, these bed designs are akin to column reactors. Two configurations can be proposed according to the direction of the electric current compared to the hydraulic flow direction. In co-current mode, they are both parallel (Figs. 10d and 10f), while in counter-current mode they are perpendicular (Figs. 10e and 10g). The co-current condition is useful for testing different porous materials in lab-scale studies (Coeuret, 2003). However, this configuration has not been adapted for a larger scale because of the low applied flow rate range. In contrast, the counter-current approach is compatible with industrial scale applications due to the possibility of arrangements in series and parallel (Coeuret, 2003). Additionally, the electrode performance is mainly governed by diffusion polarization in the fixed-bed electrode (Matsuno et al., 1996). This phenomenon is minimized in the fluidized-bed electrode due to the high mass transfer rate induced by the turbulence of the moving particles (Matsuno et al., 1996). However, the fluidized-bed reactor exhibits a number of inherent limitations. The most significant drawback is the range of potentials that are spatially

767 distributed within the bed, leading to a high heterogeneity distribution. The effective
768 resistance of the particle phase in the fluidized-bed electrode was found to be three to four
769 times greater than that of the fixed-bed device (Matsuno et al., 1996). Moreover, the
770 conditions under which the fluidized bed is operated are often unknown (Cheng et al., 2020).

771 Nevertheless, the fixed-bed presents numerous advantages over other reactor designs, such as
772 very high mass transfer intensification, a high specific area of the working electrode, and
773 feasibility of electrosorption processes for large-scale plant. This justifies why it has been
774 studied more (Fig. 9).

775

776

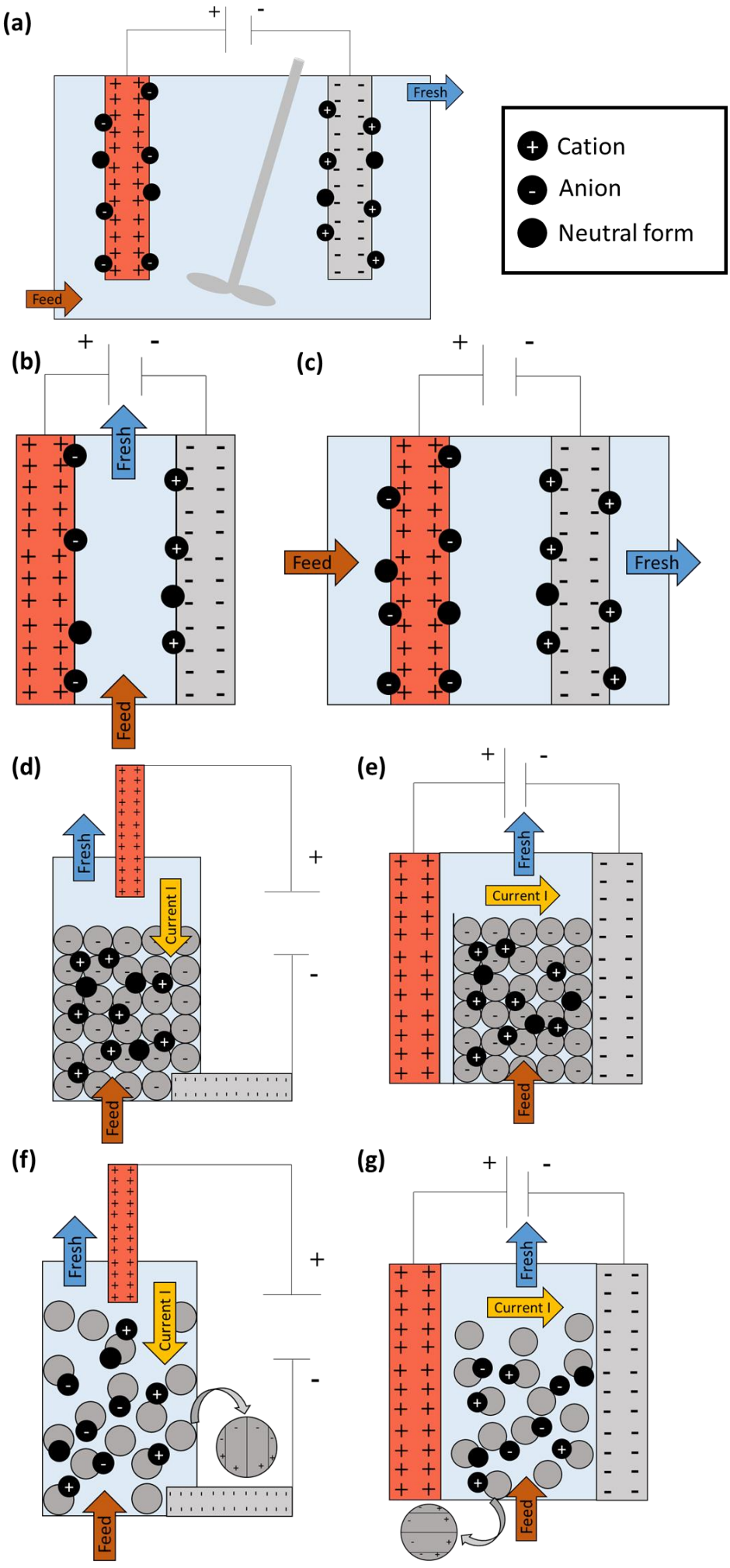
(a)
+
-
Fresh
Feed
Cation
Anion
Neutral form
(b)
Fresh
Feed
(c)
Feed
Fresh
(d)
Fresh
Current I
Feed
(e)
Fresh
Current I
Feed
(f)
Fresh
Current I
Feed
(g)
Fresh
Current I
Feed

778 **Fig. 10.** Scheme of the main electrosorption reactor designs applied in the literature: STR (a),
779 flow-by (b) and flow-through (c) parallel-plate cells, fixed-bed reactor (d, e) and fluidized-bed
780 reactor (f, g) arranged in co-current (d, f) and counter-current (e, g) configurations.

781

782 **Table 3.** Advantages and drawbacks of the different types of reactor designs implemented for
783 the electrosorption of organic compounds.

| Reactor design | Advantages | Drawbacks |
|---|---|---|
| **STR** | • Easy to manufacture<br>• Flexibility to meet different treatment objectives | • Limitations for industrial scale development<br>• High mass transfer limitations<br>• Require a higher conductivity of solutions (often needs a supporting electrolyte added)<br>• High footprint area |
| **Flow-by parallel-plate cell** | • Regenerate electrodes<br>• Offers the operational flexibility of a variable flow rate and conversion<br>• Easy control of interelectrodes gap<br>• Industrial scale applicability by implementation in stacks of cells arranged in series and parallel<br>• Good homogeneity of current and potential distributions | • Mass transfer limitations |
| **Flow-through parallel-plate cell** | • Regenerate electrodes<br>• Enhancement of mass transfer<br>• Easy control of interelectrodes gap<br>• Industrial scale applicability by | • Low flow rates range<br>• Clogging effect<br>• Pressure drop |

| | | |
|---|---|---|
| | implementation in stacks of cells arranged in series and parallel<br>• Suitable for effluent with low target compounds concentrations and low electric conductivity | |
| **Fixed-bed reactor** | • Enhancement of mass transfer<br>• Easy operating conditions<br>• High treatment capacity<br>• Industrial scale applicability<br>• High intragranular electric conductivity<br>• Suitable for effluent with low target compounds concentrations and low electric conductivity | • Higher energy requirements<br>• Clogging effect<br>• Pressure drop |
| **Fluidized-bed reactor** | • Rapid mixing rate of the bed solids<br>• Easy operating conditions<br>• Treatment of municipal and industrial wastewaters with concentrations up to a ppb level<br>• High treatment capacity<br>• Industrial scale applicability<br>• Limit clogging effect | • Higher energy requirements<br>• Low intra-granular electric conductivity<br>• High heterogeneity of current and potential distributions<br>• Low acquisition of knowledge about operating parameters (conductivity, potential, etc.) for kinetic modeling |

## 3. 7. Factors influencing the electrodesorption step

An electrodesorption step is required to recover the electrosorbed pollutants for either subsequent degradation or valorization. This further facilitates the regeneration of the porous electrode material for successive electrosorption cycles, as discussed in more detail in section 3.8 (Bain et al., 2010). It consists of reversing the electrode polarity, and the charged contaminants are then released from the interface and diffuse back into the bulk solution (McQuillan et al., 2018).

Electrode polarity and applied current or potential value are the main factors governing the electrodesorption efficiency. For instance, the desorption study of ethylenediamine from AC at a more positive potential (0 V/SCE) than for the electrosorption step (-0.5 V/SCE) provoked significant electrodesorption of the ethylenediamine back into the solution (Eisinger and Keller, 1990). However, the recovery was not complete, as it was approximately 66%, which was attributed to irreversible electrosorption of a fraction of the organic compound on the most active sites. In a similar way, thiocyanate anions were desorbed from AC by applying a negative polarization and then neutralizing or basifying the solution pH (Rong and Xien, 2009). Thus, the pH can also play a role in the desorption process according to the pKa of organic compounds. Another parameter that has been shown to influence the desorption efficiency is the solvent. The increase in methylquinolinium chloride desorption from AC was due not only to the increase in the potential from 0 mV/(Ag/saturated KCl) to 600 mV/(Ag/saturated KCl), but also to the use of methanol instead of water (Bán et al., 1998). A desorption increase of more than one hundred times was attributed to the use of methanol while keeping the applied potential lower (200 mV instead of 600 mV) (Bán et al., 1998). Methylquinolinium has a higher affinity toward methanol than water, and was preferentially desorbed with the organic solvent. This latter feature might be an approach for subsequent organic compound valorization, but not for their degradation and mineralization, as organic solvents constitute a supplementary source of pollution.

## 3. 8. Long-term efficiency of electrosorption

The regeneration and long-term efficiency of porous electrodes in a given system are also important indicators when evaluating the electrosorption performance of materials and are even more crucial in practical applications in terms of economic viability (Bayram and Ayranci, 2012a; Han et al., 2008; Yue et al., 2019). Table 4 reports successive electrosorption cycle studies with organic compounds reported in the literature. The electrosorption efficiency

decreased by 77% with the ACC electrode after three successive cycles by using a fresh solution at each cycle (Bayram and Ayranci, 2012c). In contrast, the same electrode could maintain its efficiency after the same number of cycles by reversing the polarity each time (Bayram and Ayranci, 2012a). Thus, a desorption step seems to be required before any additional electrosorption cycle in order to increase the electrode reusability and its long-term efficiency. Similarly, a 30% decrease in the ACF efficiency was observed for the first three cycles, while the electrosorption capacity remained constant during the seven subsequent cycles (Han et al., 2008). The decrease was associated with the irreversible electrosorbed fraction of organic compounds in the micropores that could not be regenerated. The microporosity of the electrode can therefore be a drawback for compound desorption and full regeneration of the material, although it is an advantage for its electrosorption. In another study, the electrosorption capacity of the prGO/SWCNT film was still as high as 1170 mg $g^{-1}$ (a 3% increase) after ten successive cycles (Yue et al., 2019). The slight increase in performance could be attributed to the enhancement of the wettability and material activation after prolonged electrode polarization.

**Table 4.** Successive electrosorption cycle studies with organic compounds reported in the literature.

| Working electrode | Organic pollutant | Number of successive cycles | Electrosorption capacity | Reference |
|---|---|---|---|---|
| prGO/SWCNTs film | MB | 10 | $1^{st}$ cycle: 1133 mg $g^{-1}$<br>$10^{th}$ cycle: 1170 mg $g^{-1}$<br>(3% increase) | (Yue et al., 2019) |
| ACF | AO7 | 10 | $1^{st}$ cycle: $RE^{*}$ = 95%<br>$10^{th}$ cycle: $RE^{*}$ = 70% | (Han et al., 2008) |

| | | | | |
|---|---|---|---|---|
| | | | (26% decrease) | |
| ACC | BA, phthalic acid and NA | 3 | 1st cycle: 15 mmol $g^{-1}$<br>3rd cycle: 15 mmol $g^{-1}$<br>(0% decrease) | (Bayram and Ayranci, 2012a) |
| ACC | BA | 4 | 1st cycle: 77.5 mmol $g^{-1}$<br>4th cycle: 5 mmol $g^{-1}$<br>(93% decrease) | (Bayram and Ayranci, 2012c) |

*RE: regeneration efficiency percentage

## 4. Modeling

In addition to the electrosorption parameters, mathematical modeling of the electrosorption process can be an effective tool for understanding the mechanisms involved, optimizing the system, predicting the efficiency, designing the reactor, and increasing the scale via dimensional analysis. Over the years, many electrosorption models have been developed, but these remain more challenging than those for adsorption reactors due to the involvement of an electric current in the transfer phenomena and reactions. The main models to improve the operating strategies for electrosorption are briefly presented from batch to continuous modes. Dimensionless numbers and scaling considerations are also discussed.

### 4. 1. Modeling in batch and continuous modes

Kinetics provides information about the residence time required for the completion of electrosorption. It constitutes the basis to determine and predict the performance of systems during the optimization step in batch mode and for the subsequent scale-up phase. The kinetic

data for electrosorption of many organic species onto carbon electrodes fit quite well with the pseudo-first-order kinetic model (Ayranci and Conway, 2001; Bayram and Ayranci, 2012b, 2012a; Han et al., 2006b). Since high surface areas of the electrodes (e.g., porous carbon materials) are used most of the time in electrosorption, the kinetic rate is often limited by the electric current and not by diffusion. This could explain the good fitting with the pseudo-first order model (Ayranci and Conway, 2001; Bayram and Ayranci, 2012b, 2012a; Han et al., 2006b).

The electrosorption isotherm remains a typical studied behavior. Numerous propositions have been made to formalize the electrosorption isotherms mathematically. The model that better fits the experimental data obtained in the electrosorption of organic compounds was the Freundlich isotherm (Biniak et al., 2013; Sahin et al., 2020; Wang et al., 2012). It can be explained by organic electrosorption onto carbon electrodes that occurs on a heterogeneous surface with a continuum of electrosorption sites with different $\Delta H_{ads}$ values.

Dynamic models, also known as breakthrough curves, have been proposed to explain the design performance and to ensure successful operation of electrosorption in continuous mode. The Adam Boharts, Thomas and Yoon-Nelson models are the main dynamic models tested in the literature regarding the electrosorption of organic compounds (Nainamalai et al., 2018).

## 4. 2. Dimensionless numbers and sizing considerations

In general, a dimensional analysis combined with a similarity assessment is commonly used to scale up electrochemical reactors by keeping dimensionless numbers constant for better and faster optimization. Table 5 summarizes the main dimensionless numbers employed in the literature regarding electrosorption processes. Three dimensionless numbers are well known to relate the hydrodynamic conditions by involving the mass-transport coefficient: the Reynolds number (*Re*), the Schmidt number (*Sc*) and the Sherwood number (*Sh*) (Cañizares et

al., 2006; Ibl, 1959; López-Bernabeu et al., 2016; Vilar and Coeuret, 1999). The mass transfer Biot number ($Bi_m$) is an additional number that allows considering the difference between the rates of the internal and external mass transfers in porous media (López-Bernabeu et al., 2016). Mass transport phenomena are important in terms of the efficiency of electrosorption systems. Numerous correlations as well as the values of dimensionless numbers have been proposed in the literature according to the type of electrochemical reactor design and to the operating conditions involved (Coeuret and Storck, 1984; Goodridge and Wright, 1983a; Newman, 1968; Pletcher and Walsh, 1993). It is important to note that in a fixed-bed reactor, the mass transport increases with the length of the bed and decreases with the diameter of the particles from the bed (Storck et al., 1975).

Another valuable parameter is the Wagner number ($Wa$), which represents the ratio between the polarization resistance of the electrode and the ohmic resistance in the electrolyte (Table 5) (Wagner, 1951). It also defines the uniformity of the current density distribution and remains an essential feature when porous electrode materials are implemented (Newman and Tobias, 1962). It is well established that a drop in the potential is expected in porous polarized materials, which induces a heterogeneous distribution within the electrode. Therefore, a compromise needs to be made between a high surface area electrode for high electrosorption capacity (i.e., a large thickness of material), while keeping the potential distribution as homogeneous as possible for a good selectivity and efficiency (i.e., a small material thickness) (Coeuret, 2003). In practice, it is preferable to implement porous electrode materials with thicknesses in the direction of a current no higher than 0.5-1 cm while maximizing the material length instead of its thickness (Coeuret, 2003; Coeuret et al., 1976; Eisinger and Keller, 1990).

Dimensionless times have also been proposed in the literature, such as $G$, $T$ and $\theta$ (Chue et al., 1993; Sene et al., 2019). $G$ refers to the competition between the electrical potential wave and

902 the sorption wave (Chue et al., 1993), whose value is compared to *T*, which is the reduced
903 time (Chue et al., 1993). When $G < T$, the final potential of the porous material is more
904 rapidly reached than the electrosorption equilibrium, while 90% of the final potential in the
905 electrode is reached at $G = T$ (Chue et al., 1993). At $T > G$, the potential is almost constant in
906 the material, and the concentration of the targeted compound(s) in the effluent begins to
907 decrease. More recently, $\theta$ has been suggested as dimensionless time to define the flow
908 regime, i.e., either the permanent or non-permanent domains (Sene et al., 2019). It allows for
909 estimating the optimal flow rate that will give an optimal charge transfer (Table 5).

910 Since fixed-bed reactors have been the most widely designed reactors applied in the literature
911 for organic electrosorption (Fig. 9), it is interesting to present a method for scaling estimation.
912 More details can be read in eminent textbooks in the field (Coeuret and Storck, 1984;
913 Goodridge and Wright, 1983a; Newman, 1968; Pletcher and Walsh, 1982). A four-time-
914 period method has been proposed to size fixed-bed reactors, namely, the residence time ($\tau_R$)
915 (Eq. 2), breakthrough time ($t_{BT}$) (Eq. 3), diffusion time ($t_D$) (Eq. 4) and $t_{dl}$ (Eq. 5) (Eisinger
916 and Keller, 1990).

917 $$\tau_R = \frac{\varepsilon_B A d}{Q_V} \quad (2)$$

918 $$t_{BT} = (q_A - q_D)\rho_B \frac{Ad}{(C_{in} - C_{out})Q_V} \quad (3)$$

919 $$t_D = \frac{(\frac{d_p}{2})^2}{2D} \quad (4)$$

920 $$t_{dl} = a\varepsilon_B C d^2 \frac{(\kappa+\sigma)}{\kappa\sigma} \quad (5)$$

921 where $\varepsilon_B$ is the bed porosity, *d* is the electrode thickness (cm), *A* is the cross-sectional area
922 ($A = H \times W$, where *H* is the bed height and *W* is the bed width) ($cm^2$), $q_D$ is the

electrodesorption (at the desorption potential) capacity (mg $g^{-1}$), $\rho_B$ is the bed density (g of material per $cm^{-3}$ of bed)), $C_{in}$ and $C_{out}$ are the targeted compound concentrations in the inlet and outlet flows, respectively (mg $cm^{-3}$), $Q_V$ is the inlet flow rate ($cm^3$ $s^{-1}$), $a$ is the interfacial area per unit void volume ($cm^2$ $cm^{-3}$), $C$ is the differential capacitance (F $cm^{-2}$), $\kappa$ and $\sigma$ are the effective electrolyte conductivity and electrical conductivity of the porous material, respectively ($(\Omega\text{-cm})^{-1}$), $d_p$ is the particle diameter (cm), and $D$ is the diffusion coefficient of the targeted compound ($cm^2$ $s^{-1}$).

For an optimal sizing, the following criteria must be considered (Eisinger and Keller, 1990):

$$t_{dl} \ll t_{BT} \quad (6)$$

$$t_D < \tau_R \ll t_{BT} \quad (7)$$

Equation 6 permits us to consider the fact that the bed needs to be completely charged at a given potential before reaching the maximum electrosorption capacity (Eisinger and Keller, 1990). Equation 7 avoids being limited by diffusion (Eisinger and Keller, 1990). At a given $A$ and $L$, the procedure is to first estimate $t_{dl}$ then $t_{BT}$, followed by the calculation of $Q$ to be implemented (Eisinger and Keller, 1990). From $Q$, $\tau_R$ is evaluated, and the condition from Eq. 7 needs to then be verified (Eisinger and Keller, 1990).

There is a need to consider these dimensionless numbers for scale-up studies with dimensional analysis as this type of consideration is lacking in literature.

**Table 5.** Main dimensionless numbers involved in the literature about the electrosorption.

| Dimensionless number | Equation | Signification |
|---|---|---|

| | | |
|---|---|---|
| $Re$ | $Re = \frac{u\, d_f}{\nu}$ | Ratio between the inertial forces and viscous forces in the liquid. It defines the hydrodynamic regime (laminar or turbulent) |
| $Sc$ | $Sc = \frac{\nu}{D_m}$ | Ratio between the momentum diffusivity and the mass diffusivity. It defines the extension of the diffusion layer |
| $Sh$ | $Sh = \frac{k_f L}{D_m}$ | Ratio between the convective mass transfer rate and the diffusion rate |
| $Bi_m$ | $Bi_m = Sh\ \frac{D_m}{D_e}$ | Ratio of the rates of internal to external mass transfers |
| $Wa$ | $Wa = \frac{\kappa}{L}\frac{d\eta}{dj}$ | Ratio between the polarization resistance of the electrode to ohmic resistance in electrolyte. It defines the uniformity of the current density distribution |
| $G$ | $G = \frac{t_{dl}}{t_{st}}$ | This defines the competition between the electrical potential wave and the sorption wave |
| $T$ | $T = \frac{t}{t_{st}}$ | Reduced time |
| $\theta$ | $\theta = \frac{t_{sc}}{t_{t0}}$ with $t_{sc} = \frac{\Delta E}{sr}$ and $t_{t0} = \frac{L}{u}$ | This defines the different flowing regimes, either the permanent or non-permanent domain |

**Abbreviations:**

$u$ is the linear velocity of the liquid through the void space of the adsorbent (m $s^{-1}$), $\nu$ is the kinematic viscosity of the solution ($m^2$ $s^{-1}$), $k_f$ denotes the external mass transfer coefficient (m $s^{-1}$), $L$ is the characteristic length (m), $D_m$ is the molecular diffusivity of the pollutant ($m^2$ $s^{-1}$), $D_e$ is the effective diffusivity ($m^2$ $s^{-1}$), $t_{dl}$ is the double layer charging time (s), $t_{st}$ is the stoichiometric time of sorption (s), $t$ is the reaction time (s), $\kappa$ is the effective electrolyte conductivity ($(\Omega\text{-m})^{-1}$), $\eta$ is the overpotential (V), $j$ is the current density (A $m^{-2}$), $t_{sc}$ is the scan time (s), $t_{t0}$ is the turnover time (s), $\Delta E$ is the potential difference (V), and $sr$ is the scan rate (V $s^{-1}$).

## 5. Current developments and future prospects

## 5.1. Current challenges to overcome

A general overview of the main factors and phenomena involved in the electrosorption efficiency is proposed and schematized in Fig. 11. This scheme allows for the identification of which parameters affect each phenomenon that then governs the electrosorption efficiency. The importance of the EDL and mass transport is influenced by most of the main parameters. Therefore, future efforts should be made to enhance both EDL and mass transport. The main output and future improvements in the electrosorption process efficiency are addressed as follows:

- Electrode material: The high specific surface area of the material is not sufficient to obtain a high electrosorption capacity since the pore size appears to also be a crucial parameter. The presence of mesopores tends to improve the efficiency. Therefore, the specific surface area and the pore size distribution of materials should be determined prior to experiments to ensure a maximum electrosorption of the pollutants. Moreover, the material conductivity and wettability should not be neglected in the mechanisms. Material stability and reusability are other essential criteria for long-term use in practical applications. Existing studies lack life span and regeneration tests, which are representative of real conditions.
- Electrode potential and polarity: An optimal electrode potential is required for optimal electrosorption, while values that are too high or too low lead to faradaic reactions that need to be avoided. The electrode polarity plays a role in the electrosorption efficiency according to the types of targeted compounds, but the porous material can be damaged if it does not support either oxidative or reductive potentials. Carbon-based materials have been widely employed in electrosorption, although they can be easily corroded as anodes.

Therefore, caution should be taken in the applied conditions to preserve the lifetime of the electrode material.

- Electrolyte concentration and properties: Although an increase in the electrolyte concentration increases the solution conductivity and therefore decreases the ohmic resistance, co-sorption with either inorganic or organic compounds occurs. Thus, it can decrease the electrosorption of the targeted compounds as well as the selectivity. In addition, the pKa of organic compounds can influence their electrosorption efficiency and selectivity according to the solution pH. However, there is an important need to operate with more complex matrices until actual wastewater is tested in order to better assess the viability of the technique in practical conditions. Moreover, high concentrations of supporting electrolytes have often been added, while they should be avoided in a wastewater treatment context.
- Reactor design: A fixed-bed reactor has been implemented the most extensively, which is ascribed to the high mass transfer, the high specific area of the porous electrode and the scale-up ability. A still pressure drop and clogging effect can occur with this type of reactor. A less conventional design that was recently proposed could also be tested by combining micro-reactors with macro-reactors to avoid these drawbacks (Mousset, 2020). Moreover, an adapted design should be used to operate with a low solution conductivity without adding a supporting electrolyte.
- Modeling: Interface phenomena represented by EDL theory are still not well understood under specific conditions (e.g., highly concentrated electrolytes and dense electrolytes). DFT models are gaining an increasing interest; however, their single use induces scale-level heterogeneity: the atomic level at the electrode surface is considered, while a simple continuum model for the electrolyte is taken into account without considering the discrete form (e.g., dipoles) (Schmickler, 2020). Complete models of the interfaces should describe electrons, solvents, ions and interactions between one another (Schmickler,

2020). Coupling DFT with molecular dynamics (Oleinick et al., 2019) or combining DFT with a reference interaction site model (Schmickler, 2020) have recently been suggested to obtain a more complete overview of the mechanisms at the interface. Moreover, kinetic models in either batch or continuous modes should incorporate the matrix effect, the transport phenomena, and the physico-chemical properties of compounds on the electrosorption rates and yields of organics to better understand and predict the efficiency. This will further benefit scale-up studies that include dimensional analysis and a similarity assessment. This is an important tool to reach higher technology readiness level.

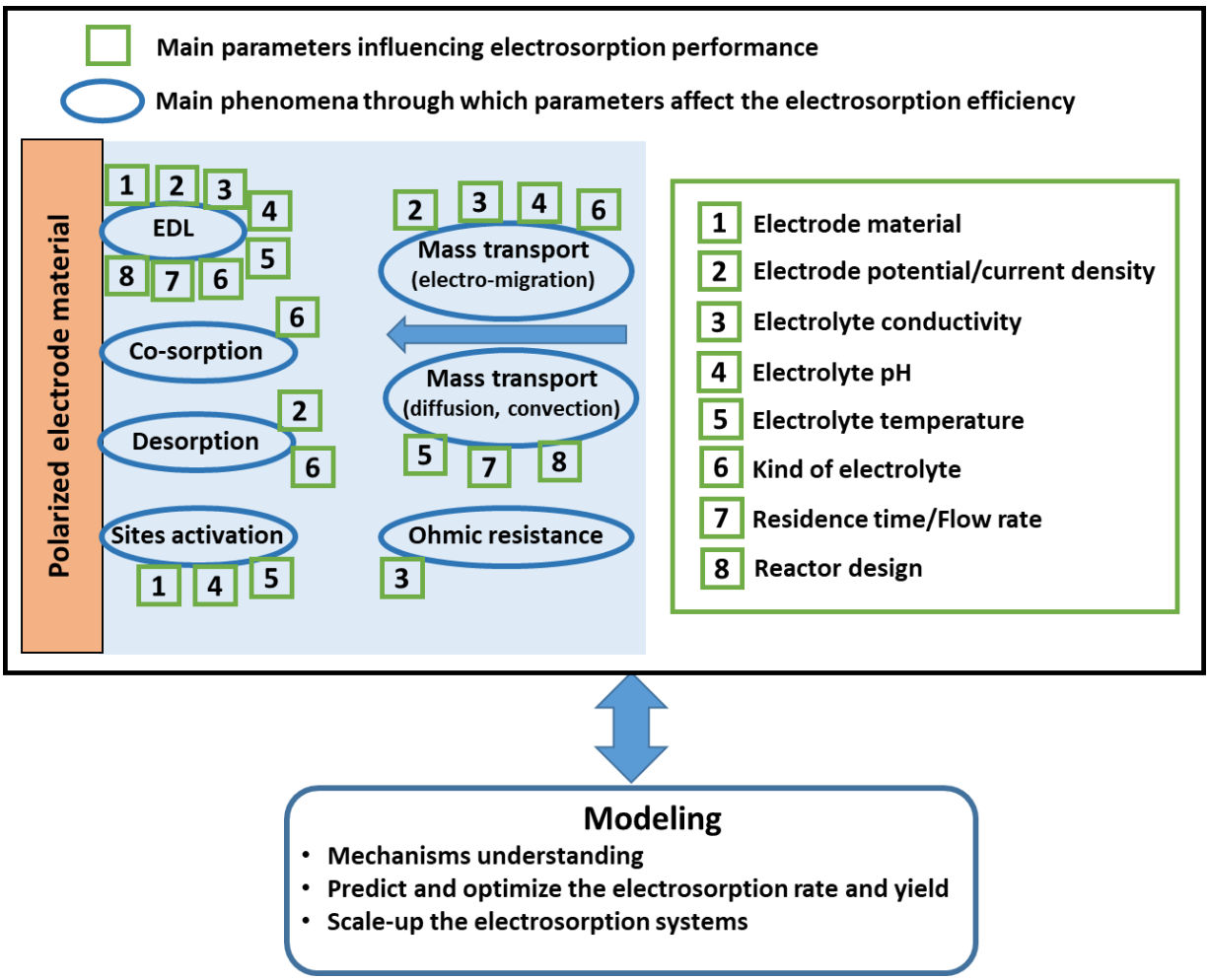


**Fig. 11.** General overview of the main parameters and phenomena involved in the electrosorption efficiency associated with a modeling approach.

## 5.2. Emerging processes combinations with electrosorption

Electrosorption was initially proposed for separation purposes to remove selected compounds from wastewater, but the treatment strategy could be extended. The recovery of added-value organic compounds in wastewater would be another option after optimizing the electrosorption and electrodesorption conditions for optimal selectivity. An alternative strategy would be to combine electrosorption as a separation technology with a degradation process, which is required for a more integrated treatment of the wastewater. Many researchers studied emerging processes (photocatalytic, electrooxidation, electrically conductive ultrafiltration, electro-Fenton, advanced oxidation processes, electrocatalysis, peroxi-coagulation, solid-phase microextraction,...) combination with electrosorption using several kinds of electrode materials for the removal of various organic pollutants (Ayoubi-Feiz et al., 2018, 2014b, 2014a; Chai et al., 2021; Chen et al., 2018; Fan et al., 2018; Jin et al., 2011; Mantel et al., 2021; Nie et al., 2019; Wang et al., 2013; Xu et al., 2019; Yang et al., 2021). Table 6 provides an overview of the main studies in literature illustrating these processes combination. It was noticed that the photoelectrocatalysis has been the most employed process in combination with electrosorption for the removal of nonylphenol (Fan et al., 2018), alizarin red (Jin et al., 2011), diazinon (Ayoubi-Feiz et al., 2018), reactive yellow 39 (Ayoubi-Feiz et al., 2014b) and lanasol red 5B (Ayoubi-Feiz et al., 2014a). Electrooxidation/electroreduction processes have particularly demonstrated a high ability to remove pollutants from wastewater (Garcia-Rodriguez et al., 2020; Martinez-Huitle et al., 2015; Moreira et al., 2017; Mousset et al., 2018c; Mousset and Doudrick, 2020; Trellu et al., 2021) by implementing a boron-doped diamond anode with a high $O_2$ evolution overvoltage (Mousset et al., 2019b; Nidheesh et al., 2019). The degradation and mineralization efficiency

is notably due to the involvement of hydroxyl radicals that have a very high reactivity and quasi non-selectivity toward organic compounds (Brillas et al., 2009; Mousset et al., 2018a; Panizza and Cerisola, 2009). In combination with electrosorption techniques, the global performance is enhanced by maintaining a high degradation yield. For instance, electrooxidation combined with electrosorption was tested in the removal of BA (Chen et al., 2018), acyclovir and phenol (Nie et al., 2019), while the combination with peroxi-coagulation was investigated for the removal of Orange II (Yang et al., 2021). In addition, Chai et al. (2021) investigated the combination of electro-Fenton with electrosorption in the removal of toluene and trichloromethane (Chai et al., 2021). The authors used a flow-through electro-Fenton treatment (anode: pure iron and cathode: Ti mesh), followed by the electrosorption treatment (anode and cathode were ACF). The removal efficiency is 96% for COD, 98% for $NH_3$-N, and 46% for salinity under the optimal conditions (voltage intensity of 1.5 V, initial pH of 4, plate spacing of 1 cm, flow rate of 40 mL $min^{-1}$, $H_2O_2$ concentration of 50 mM). A similar study was performed by Wang et al. (2013) with imidacloprid (Wang et al., 2013). Another advantage of such combinations is the synergy obtained by limiting the amount of potentially formed toxic byproducts (e.g., chlorate and perchlorate), as recently published (Norra and Radjenovic, 2021). Therefore, these combinations seem to offer promising results in the near future for a reliable development at a real scale.

1059 **Table 6.** Summary of the main emerging processes combinations with electrosorption applied in treatment of organic pollutants.

| Combined process with electrosorption | Working electrode | Organic pollutant | Efficiency | Reference |
|---|---|---|---|---|
| Photoelectrocatalysis | $Bi_2WO_6$/Carbon aerogel | Nonylphenol | Combined processes: 99% | (Fan et al., 2018) |
| Photoelectrocatalysis | Nano N-$TiO_2$/graphene/titanium grid sheet | Diazinon | Electrosorption: 24% Photocatalytic: 28% | (Ayoubi-Feiz et al., 2018) |
| Photoelectrocatalysis | α-$Fe_2O_3$/$TiO_2$/AC plate nanocomposite | Reactive yellow 39 | Adsorption: 28% Electrosorption: 43% Photocatalytic: 38% | (Ayoubi-Feiz et al., 2014b) |
| Electro-Fenton | Iron oxide grown AC aerogel | Imidacloprid | Combined processes: 90% | (Wang et al., 2013) |
| Electro-Fenton | AC felt | Toluene and trichloromethane | Combined process: 96% of COD removal | (Chai et al., 2021) |

| | | | | |
|---|---|---|---|---|
| Electrooxidation | MWCNTs/peroxydisulfate | Acyclovir and phenol | Combined processes:<br>Acyclovir: 97%<br>Phenol: 61% | (Nie et al., 2019) |
| Electrooxidation | $TiO_2$-NTs/3D-$SnO_2$-Sb electrode | BA | Combined processes: 89% | (Chen et al., 2018) |
| Peroxi-coagulation | ACF and iron sheet | Orange II | Combined processes:<br>Removal efficiency: 93%<br>Removal capacity: 1043 mg $g^{-1}$ | (Yang et al., 2021) |
| Electrically conductive ultrafiltration | Conductive membrane | River natural organic matter, Hohloh lake natural organic matter, humic acid and brilliant blue ionic dye | Combined processes:<br>River natural organic matter: 70%<br>Hohloh lake natural organic matter: 75%<br>Humic acid: 93%<br>Brilliant Blue ionic dye: 99% | (Mantel et al., 2021) |
| Electrocatalysis | Layer-by-layer CNT/$PbO_2$ | Sodium pentachlorophenate | Combined processes: 74% | (Xu et al., 2019) |
| Photocatalysis | Nanosized $TiO_2$/AC plate electrode | Lanasol red 5B | Photocatalytic: 66%<br>Combined processes: 86% | (Ayoubi-Feiz et al., 2014a) |

| | | | | |
|---|---|---|---|---|
| Photocatalysis | $TiO_2$/carbon aerogel | Alizarin red | Electrosorption: 31%<br>Combined processes: 97% | (Jin et al., 2011) |

## Acknowledgements

This work was funded by the PHC TOUBKAL 2019 Project (French-Morocco bilateral program) grant number: 41525VG. The authors would like to thank the Laboratoire Réactions et Génie des Procédés (LRGP), CNRS/Université de Lorraine (France) for the scientific support to this work and National Center for Studies and Research on Water and Energy (Cadi Ayyad University_Morocco).

# References


Adnan, F.H., Mousset, E., Pontvianne, S., Pons, M., 2021a. Mineral cathodic electro-precipitation and its kinetic modelling in thin-film microfluidic reactor during advanced electro-oxidation process. Electrochim. Acta 387, 138487. https://doi.org/10.1016/j.electacta.2021.138487

Adnan, F.H., Pons, M.-N., Mousset, E., 2021b. Mass transport evolution in microfluidic thin film electrochemical reactors: New correlations from millimetric to submillimetric interelectrode distances. Electrochem. commun. 130, 107097. https://doi.org/10.1016/j.elecom.2021.107097

Ahmad, T., Guria, C., Mandal, A., 2020. Journal of Water Process Engineering A review of oily wastewater treatment using ultrafiltration membrane : A parametric study to enhance the membrane performance. J. Water Process Eng. 36, 101289. https://doi.org/10.1016/j.jwpe.2020.101289

Alagesan, J., Jaisankar, M., Muthuramalingam, S., Mousset, E., Chellam, P.V., 2021. Influence of number of azo bonds and mass transport limitations towards the elimination capacity of continuous electrochemical process for the removal of textile industrial dyes. Chemosphere 262. https://doi.org/10.1016/j.chemosphere.2020.128381

Alencherry, T., A.R., N., Ghosh, S., Daniel, J., Venkataraghavan, R., 2017. Effect of increasing electrical conductivity and hydrophilicity on the electrosorption capacity of activated carbon electrodes for capacitive deionization. Desalination 415, 14–19. https://doi.org/10.1016/j.desal.2017.04.001

Ania, C.O., Béguin, F., 2007. Mechanism of adsorption and electrosorption of bentazone on activated carbon cloth in aqueous solutions. Water Res. 41, 3372–3380. https://doi.org/10.1016/j.watres.2007.03.031

1091 Ayoubi-Feiz, B., Aber, S., Khataee, A., Alipour, E., 2014a. Electrosorption and photocatalytic
1092 one-stage combined process using a new type of nanosized $TiO_2$ /activated charcoal
1093 plate electrode. Environ. Sci. Pollut. Res. Int. 21, 8555–64.
1094 https://doi.org/10.1007/s11356-014-2777-z

1095 Ayoubi-Feiz, B., Aber, S., Khataee, A., Alipour, E., 2014b. Preparation and application of α-
1096 Fe2O3/TiO2/activated charcoal plate nanocomposite as an electrode for electrosorption-
1097 assisted visible light photoelectrocatalytic process. J. Mol. Catal. A Chem. 395, 440–448.
1098 https://doi.org/10.1016/j.molcata.2014.09.006

1099 Ayoubi-Feiz, B., Mashhadizadeh, M.H., Sheydaei, M., 2018. Preparation of reusable nano N-
1100 TiO2/graphene/titanium grid sheet for electrosorption-assisted visible light
1101 photoelectrocatalytic degradation of a pesticide: Effect of parameters and neural network
1102 modeling. J. Electroanal. Chem. 823, 713–722.
1103 https://doi.org/10.1016/j.jelechem.2018.07.020

1104 Ayranci, E., Conway, B.E., 2001. Removal of phenol, phenoxide and chlorophenols from
1105 waste-waters by adsorption and electrosorption at high-area carbon felt electrodes 513,
1106 100–110.

1107 Bagheri, H., Fakhri, H., Ghahremani, R., Karimi, M., Madrakian, T., Afkhami, A., 2020.
1108 Nanomaterial-based adsorbents for wastewater treatment, Smart Nanocontainers.
1109 Elsevier Inc. https://doi.org/10.1016/b978-0-12-816770-0.00028-9

1110 Bain, E.J., Calo, J.M., Spitz-Steinberg, R., Kirchner, J., Axén, J., 2010.
1111 Electrosorption/electrodesorption of arsenic on a granular activated carbon in the
1112 presence of other heavy metals. Energy and Fuels 24, 3415–3421.
1113 https://doi.org/10.1021/ef901542q

1114 Bán, A., Schäfer, A., Wendt, H., 1998. Fundamentals of electrosorption on activated carbon

for wastewater treatment of industrial effluents. J. Appl. Electrochem. 28, 227–236. https://doi.org/10.1023/A:1003247229049

Bard, A.J., Faulkner, L.R., 2001. Electrochemical methods - Fundamentals and Applications, 2nd Ed. ed. John Wiley & Sons, Inc. https://doi.org/10.1016/B978-0-12-381373-2.00056-9

Bayram, E., 2016. Electrosoption of Aromatic Organic Acids From Aqueous Solutions Onto Granular Activated Carbon Electrodes for Water Purification. Hacettepe J. Biol. Chem. 3, 273–273. https://doi.org/10.15671/hjbc.20164420570

Bayram, E., Ayranci, E., 2012a. Structural effects on electrosorptive behavior of aromatic organic acids from aqueous solutions onto activated carbon cloth electrode of a flow-through electrolytic cell. J. Electroanal. Chem. 683, 14–20. https://doi.org/10.1016/j.jelechem.2012.07.028

Bayram, E., Ayranci, E., 2012b. Electrosorption based wastewater treatment system using activated carbon cloth electrode: Electrosorption of benzoic acid from a flow-through electrolytic cell. Sep. Purif. Technol. 86, 113–118. https://doi.org/10.1016/j.seppur.2011.10.032

Bayram, E., Ayranci, E., 2012c. Electrosorption based waste water treatment system using activated carbon cloth electrode: Electrosorption of benzoic acid from a flow-through electrolytic cell. Sep. Purif. Technol. 86, 113–118. https://doi.org/10.1016/j.seppur.2011.10.032

Bayram, E., Kizil, Ç., Ayranci, E., 2018. Flow-through electrosorption process for removal of 2,4-D pesticide from aqueous solutions onto activated carbon cloth fixed-bed electrodes. Water Sci. Technol. 77, 848–854. https://doi.org/10.2166/wst.2017.598

Bazant, M.Z., Storey, B.D., Kornyshev, A.A., 2011. Double layer in ionic liquids:

1139 Overscreening versus crowding. Phys. Rev. Lett. 106.
1140 https://doi.org/10.1103/PhysRevLett.106.046102

1141 Belarbi, Z., Sotta, B., Makhloufi, L., Tribollet, B., Gamby, J., 2016. Modelling of delay effect
1142 of calcium carbonate deposition kinetics on rotating disk electrode in the presence of
1143 green inhibitor. Electrochim. Acta 189, 118–127.
1144 https://doi.org/10.1016/j.electacta.2015.12.089

1145 Bergmann, M.E.H., Rollin, J., Iourtchouk, T., 2009. The occurrence of perchlorate during
1146 drinking water electrolysis using BDD anodes. Electrochim. Acta 54, 2102–2107.
1147 https://doi.org/10.1016/j.electacta.2008.09.040

1148 Biniak, S., Świątkowski, A., Pakuła, M., Sankowska, M., Kuśmierek, K., Trykowski, G.,
1149 2013. Cyclic voltammetric and FTIR studies of powdered carbon electrodes in the
1150 electrosorption of 4-chlorophenols from aqueous electrolytes. Carbon N. Y. 51, 301–312.
1151 https://doi.org/10.1016/j.carbon.2012.08.057

1152 Brillas, E., Sirés, I., Oturan, M.A., 2009. Electro-Fenton process and related electrochemical
1153 technologies based on Fenton's reaction chemistry. Chem. Rev. 109, 6570–6631.
1154 https://doi.org/10.1007/s00894-008-0358-0

1155 Brito, C.D.N., de Araújo, D.M., Martínez-Huitle, C.A., Rodrigo, M.A., 2015. Understanding
1156 active chlorine species production using boron doped diamond films with lower and
1157 higher sp3/sp2 ratio. Electrochem. commun. 55, 34–38.
1158 https://doi.org/10.1016/j.elecom.2015.03.013

1159 Brummer, S.B., Ford, J.I., Turner, M.J., 1965. The adsorption and oxidation of hydrocarbons
1160 on noble metal electrodes. I. Propane adsorption on smooth platinum electrodes. J. Phys.
1161 Chem. 69, 3424–3433. https://doi.org/10.1021/j100894a031

1162 Butler, J.A.., Armstrong, G., 1933. The kinetics of electrode processes. Part II.—Reversible

reduction and oxidation processes. Proceeding R. Soc. A 139, 406–416. https://doi.org/10.1524/zpch.1972.80.1_2.110a

Cañizares, P., Marcos, I.F. De, Rodrigo, M.A., Lobato, J., 2006. Measurement of Mass-Transfer Coefficients by an Electrochemical Technique. J. Chem. Educ. 83, 1204–1207. https://doi.org/10.1021/ed083p1204

Chabot, V., Higgins, D., Yu, A., Xiao, X., Chen, Z., Zhang, J., 2014. A review of graphene and graphene oxide sponge: material synthesis and applications to energy and the environment. Energy Environ. Sci. 7, 1564. https://doi.org/10.1039/c3ee43385d

Chai, X., He, Y., Ying, D., Jia, J., Sun, T., 2007. Electrosorption-enhanced solid-phase microextraction using activated carbon fiber for determination of aniline in water. J. Chromatogr. A 1165, 26–31. https://doi.org/10.1016/j.chroma.2007.07.048

Chai, Y., Qin, P., Wu, Z., Bai, M., Li, W., Pan, J., Cao, R., Chen, A., Jin, D., Peng, C., 2021. A coupled system of flow-through electro-Fenton and electrosorption processes for the efficient treatment of high-salinity organic wastewater. Sep. Purif. Technol. 267, 118683. https://doi.org/10.1016/j.seppur.2021.118683

Chang, L., Li, J., Duan, X., Liu, W., 2015. Porous carbon derived from Metal-organic framework (MOF) for capacitive deionization electrode. Electrochim. Acta 176, 956–964. https://doi.org/10.1016/j.electacta.2015.07.130

Chang, L., Zhou, Y., Duan, X., 2014. Kinetics and equilibrium studies on the electrosorption of anions with activated carbon electrodes. Desalin. Water Treat. 52, 6549–6555. https://doi.org/10.1080/19443994.2013.816873

Chapman, D.L., 1913. A contribution to the theory of electrocapillary. Philos. Mag. 25, 475–481. https://doi.org/10.1016/0304-3975(85)90090-8

Chen, Y., Tu, Y., Bai, Y., Li, J., Lu, J., 2018. Electrosorption enhanced electrooxidation of a model organic pollutant at 3D SnO2-Sb electrode in superimposed pulse current mode. Chemosphere 195, 63–69. https://doi.org/10.1016/j.chemosphere.2017.12.074

Cheng, J., Yang, H., Fan, C., Li, R., Yu, X., Li, H., 2020. Review on the applications and development of fluidized bed electrodes. J. Solid State Electrochem. 24, 2199–2217. https://doi.org/10.1007/s10008-020-04786-w

Chmiola, J., Yushin, G., Gogotsi, Y., Portet, C., Simon, P., Taberna, P.L., 2006. Anomalous increase in carbon at pore sizes less than 1 nanometer. Science (80-. ). 313, 1760–1763. https://doi.org/10.1126/science.1132195

Chue, K.T., Grévillot, G., Tondeur, D., 1993. Electrosorption an Activated Carbon Bed. Stud. Surf. Sci. Catal. 80, 97–104. https://doi.org/10.1016/S0167-2991(08)63503-X

Coeuret, F., 2003. Ingénierie des procédés électrochimiques. Ellipses, Paris (France).

Cœuret, F., 1993. A flow-through porous electrode patented 100 years ago: the Hulin process. J. Appl. Electrochem. 23, 853–855. https://doi.org/10.1007/BF00249961

Coeuret, F., Hutin, D., Gaunand, A., 1976. Study of the effectiveness of fixed flow-through electrodes. J. Appl. Electrochem. 6, 417–423. https://doi.org/10.1007/BF00616541

Coeuret, F., Legrand, J., 1985. Mass transfer at the electrodes of the "falling-film cell." J. Appl. Electrochem. 15, 181–190.

Coeuret, F., Storck, A., 1984. Eléments de génie électrochimique, 1st Ed. ed. Tec & Doc, Paris (France).

Conway, B.E., 1999. Theoretical Treatment and Modeling of the Double Layer at Electrode Interfaces, in: Electrochemical Supercapacitors. pp. 125–168. https://doi.org/10.1007/978-1-4757-3058-6_7

Crini, G., Lichtfouse, E., 2019. Advantages and disadvantages of techniques used for wastewater treatment. Environ. Chem. Lett. 17, 145–155. https://doi.org/10.1007/s10311-018-0785-9

Crini, G., Lichtfouse, E., Wilson, L.D., Morin-Crini, N., 2019. Conventional and non-conventional adsorbents for wastewater treatment. Environ. Chem. Lett. 17, 195–213. https://doi.org/10.1007/s10311-018-0786-8

Dai, G., Zhang, L., Liao, Y., Shi, Y., Xie, J., Lei, F., Fan, L., 2020. Multi-Scale Model for Describing the Effect of Pore Structure on Carbon-Based Electric Double Layer. J. Phys. Chem. C 124, 3952–3961. https://doi.org/10.1021/acs.jpcc.9b10587

Damaskin, B.B., 2011. Modeling of co-adsorption of cations and anions localized in different layers of the dense part of electrical double layer under the conditions of linear charge dependence of the adsorption energy. Russ. J. Electrochem. 47, 988–994. https://doi.org/10.1134/S1023193511090047

Damaskin, B.B., 2009. Mechanism of coadsorption of two organic substances on electrodes at strong attractive interaction between their molecules in the adsorption layer. Russ. J. Electrochem. 45, 241–245. https://doi.org/10.1134/S102319350903001X

Damaskin, B.B., 2008. Modeling of synergism effect at different orientation of co-adsorbing molecules. Russ. J. Electrochem. 44, 1313–1319. https://doi.org/10.1134/S102319350812001X

Damaskin, B.B., Baturina, O.A., 2001a. Some anomalies in coadsorption of two organic substances due to differences in molecular interaction of species undergoing coadsorption. Russ. J. Electrochem. 37, 1292–1299. https://doi.org/10.1023/A:1013239813826

Damaskin, B.B., Baturina, O.A., 2001b. Simulating coadsorption of surface active anions and

organic molecules capable of forming two-dimensional condensed layers on the electrode. Elektrokhimiya 37, 141–147.

Damaskin, B.B., Baturina, O.A., 2001c. Simulation of coadsorption of inorganic ions and organic molecules on electrodes. Elektrokhimiya 37, 87–94.

Damaskin, B.B., Baturina, O.A., 1999. Co-adsorption of anions and low-adsorbing cations within the Alekseev-Popov-Kolotyrkin model. Russ. J. Electrochem. 35(11), 1182–1185.

Damaskin, B.B., Petrii, O.A., 2011. Historical development of theories of the electrochemical double layer. J. Solid State Electrochem. 15, 1317–1334. https://doi.org/10.1007/s10008-011-1294-y

Damaskin, B.B., Safonov, V.A., Safonov, N. V., 2003. Adsorption of an Organic Compound in Two Different Positions: Simulation Taking into Account All Three Parameters of Intermolecular Interaction. Russ. J. Electrochem. 39, 814–819. https://doi.org/10.1023/A:1024898607524

Du, X., Oturan, M.A., Zhou, M., Belkessa, N., Su, P., Cai, J., Trellu, C., Mousset, E., 2021. Nanostructured electrodes for electrocatalytic advanced oxidation processes: From materials preparation to mechanisms understanding and wastewater treatment applications. Appl. Catal. B Environ. 296, 120332. https://doi.org/10.1016/j.apcatb.2021.120332

Eisinger, R.S., 1983. Separation by Electrosorption of Organic Compounds in a Flow-Through Porous Electrode. J. Electrochem. Soc. 130, 93. https://doi.org/10.1149/1.2119689

Eisinger, R.S., Alkire, R.C., 1980. Electrosorption of β-naphthol on graphite. Journal of Electroanalytical Chemistry and Interfacial Electrochemistry 112, 327–337.

Eisinger, R.S., Keller, G.E., 1990. Electrosorption: A case study on removal of dilute organics from water. Environ. Prog. 9, 235–244. https://doi.org/10.1002/ep.670090418

Fan, L., Liu, Y., Xiong, J., White, H.S., Chen, S., 2014. Electron-transfer kinetics and electric double layer effects in nanometer-wide thin-layer cells. ACS Nano 8, 10426–10436. https://doi.org/10.1021/nn503780b

Fan, Z., Shi, H., Zhao, H., Cai, J., Zhao, G., 2018. Application of carbon aerogel electrosorption for enhanced Bi2WO6 photoelectrocatalysis and elimination of trace nonylphenol. Carbon N. Y. 126, 279–288. https://doi.org/10.1016/j.carbon.2017.10.009

Feng, G., Qiao, R., Huang, J., Sumpter, B.G., Meunier, V., 2010. Ion distribution in electrified micropores and its role in the anomalous enhancement of capacitance. ACS Nano 4, 2382–2390. https://doi.org/10.1021/nn100126w

Folaranmi, G., Bechelany, M., Sistat, P., Cretin, M., Zaviska, F., 2020. Towards electrochemical water desalination techniques: A review on capacitive deionization, membrane capacitive deionization and flow capacitive deionization. Membranes (Basel). 10. https://doi.org/10.3390/membranes10050096

Foo, K.Y., Hameed, B.H., 2009. A short review of activated carbon assisted electrosorption process: An overview, current stage and future prospects. J. Hazard. Mater. https://doi.org/10.1016/j.jhazmat.2009.05.057

Frackowiak, E., 2001. Carbon materials for the electrochemical storage of energy in capacitors. Carbon N. Y. 39, 937–950.

Frumkin, A., Damaskin, B., Petrii, O., 1974. On the charge transfer in the process of adsorption at the electrode/solution interface. Electroanal. Chem. Interfacial Electrochem. 53, 57–65.

Ganzenko, O., Huguenot, D., van Hullebusch, E.D., Esposito, G., Oturan, M.A., 2014. Electrochemical advanced oxidation and biological processes for wastewater treatment: a review of the combined approaches. Environ. Sci. Pollut. Res. Int. 21, 8493–524. https://doi.org/10.1007/s11356-014-2770-6

Gao, T., Li, H., Zhou, F., Gao, M., Liang, S., Luo, M., 2019. Mesoporous carbon derived from ZIF-8 for high efficient electrosorption. Desalination 451, 133–138. https://doi.org/10.1016/j.desal.2017.06.021

Garcia-Rodriguez, O., Mousset, E., Olvera-Vargas, H., Lefebvre, O., 2020. Electrochemical treatment of highly concentrated wastewater: A review of experimental and modeling approaches from lab- to full-scale. Crit. Rev. Environ. Sci. Technol. 0, 1–70. https://doi.org/10.1080/10643389.2020.1820428

Geim, A., Novoselov, K., 2007. The rise of graphene. Nat. Mater. 6, 183–191.

Gerçel, Ö., 2016. Removal of textile dye from aqueous solution by electrochemical method. Sep. Sci. Technol. 51, 711–717. https://doi.org/10.1080/01496395.2015.1088870

Gileadi, E., 1966. Electrosorption of uncharged molecules on solid electrodes. J. Electroanal. Chem. 11, 137–151. https://doi.org/10.1016/0022-0728(66)80073-6

Gileadi, E., Duić, L., Bockris, J.O.M., 1968. A comparison of radiotracer and electrochemical methods for the measurement of the electrosorption of organic molecules. Electrochim. Acta 13, 1915–1935. https://doi.org/10.1016/0013-4686(68)80103-3

Gileadi, E., Rubin, B.T., Bockris, J.O.M., 1965. Electrosorption of ethylene on platinum as a function of potential, concentration, and temperature. J. Phys. Chem. 69, 3335–3345. https://doi.org/10.1021/j100894a019

Goodridge, F., Wright, A.R., 1983a. Porous flow-through and fluidized-bed electrodes, in: In

Comprehensive Treatise of Electrochemistry (Pp. 393-443). Springer, Boston, MA. pp. 393–443.

Goodridge, F., Wright, A.R., 1983b. Porous flow-through and fluidized-bed electrodes, in: Comprehensive Treatise of Electrochemistry. pp. 393–443.

Gouy, M., 1910. Charge électrique à la surface d'un électrolyte. J. Phys 9, 457–468.

Grahame, D.C., 1947. The electrical double layer and the theory of electrocapillarity. Chem. Rev. 41, 441–501. https://doi.org/10.1021/cr60130a002

Grahame, D.C., 1946. Properties of the Electrical Double Layer at a Mercury Surface. II. The Effect of Frequency on the Capacity and Resistance of Ideal Polarized Electrodes. J. Am. Chem. Soc. 68, 301–310. https://doi.org/10.1021/ja01206a045

Han, Y., Quan, X., Chen, S., Zhao, H., Cui, C., Zhao, Y., 2006a. Electrochemically enhanced adsorption of aniline on activated carbon fibers. Sep. Purif. Technol. 50, 365–372. https://doi.org/10.1016/j.seppur.2005.12.011

Han, Y., Quan, X., Chen, S., Zhao, H., Cui, C., Zhao, Y., 2006b. Electrochemically enhanced adsorption of phenol on activated carbon fibers in basic aqueous solution. J. Colloid Interface Sci. 299, 766–771. https://doi.org/10.1016/j.jcis.2006.03.007

Han, Y., Quan, X., Ruan, X., Zhang, W., 2008. Integrated electrochemically enhanced adsorption with electrochemical regeneration for removal of acid orange 7 using activated carbon fibers. Sep. Purif. Technol. 59, 43–49. https://doi.org/10.1016/j.seppur.2007.05.026

Hazourli, S., Bonnecaze, G., Astruc, M., 1996. Adsorption et electrosorption de composes organiques sur charbon actif en grains partie i - influence du potentiel imposé et du nombre de cycles adsorption and electrosorption of organic compounds on granular

activated carbon part i - influence of applied. Environ. Technol. (United Kingdom) 17, 1275–1283. https://doi.org/10.1080/09593330.1996.9618457

He, F., Hemmatifar, A., Bazant, M.Z., Hatton, T.A., 2020. Selective adsorption of organic anions in a flow cell with asymmetric redox active electrodes. Water Res. 182, 115963. https://doi.org/10.1016/j.watres.2020.115963

Heiland, W., Gileadi, E., Bockris, J.O.M., 1966. Kinetic and thermodynamic aspects of the electrosorption of benzene on platinum electrodes. J. Phys. Chem. 70, 1207–1216. https://doi.org/10.1021/j100876a040

Helmholtz, H. von, 1879. Studien über electrische Grenzschichten. Ann. der Phys. und Chemie 243, 22–382.

Henstridge, M.C., Dickinson, E.J.F., Compton, R.G., 2010. On the estimation of the diffuse double layer of carbon nanotubes using classical theory: Curvature effects on the Gouy-Chapman limit. Chem. Phys. Lett. 485, 167–170. https://doi.org/10.1016/j.cplett.2009.12.034

Holubowitch, N., Omosebi, A., Gao, X., Landon, J., Liu, K., 2017. Quasi-Steady-State Polarization Reveals the Interplay of Capacitive and Faradaic Processes in Capacitive Deionization. ChemElectroChem 4, 2404–2413. https://doi.org/10.1002/celc.201700082

Hou, C.H., Huang, J.F., Lin, H.R., Wang, B.Y., 2012. Preparation of activated carbon sheet electrode assisted electrosorption process. J. Taiwan Inst. Chem. Eng. 43, 473–479. https://doi.org/10.1016/j.jtice.2011.12.003

Huang, J., Sumpter, B.G., Meunier, V., 2008. Theoretical model for nanoporous carbon supercapacitors. Angew. Chemie - Int. Ed. 47, 520–524. https://doi.org/10.1002/anie.200703864

Hulin, P.L., 1893. Procédés et appareil électrolytiques pour la séparation immédiate des produits d'électrolyse liquides ou dissous.

Huong Le, T.X., Dumée, L.F., Lacour, S., Rivallin, M., Yi, Z., Kong, L., Bechelany, M., Cretin, M., 2019. Hybrid graphene-decorated metal hollow fibre membrane reactors for efficient electro-Fenton - Filtration co-processes. J. Memb. Sci. 587, 117182. https://doi.org/10.1016/j.memsci.2019.117182

Ibl, N., 1959. The use of dimensionless groups in electrochemistry. Electrochim. Acta 1, 117–129. https://doi.org/10.1016/0013-4686(59)85001-5

Jayson, G.G., Sangster, J.A., Thompson, G., Wilkinson, M.C., 1987. Adsorption and electrosorption of mercury(II) acetate onto activated charcoal cloth from aqueous solution. Carbon N. Y. 25, 523–531. https://doi.org/10.1016/0008-6223(87)90193-X

Jin, Y., Wu, M., Zhao, G., Li, M., 2011. Photocatalysis-enhanced electrosorption process for degradation of high-concentration dye wastewater on TiO2/carbon aerogel. Chem. Eng. J. 168, 1248–1255. https://doi.org/10.1016/j.cej.2011.02.026

Johnson, A.M., Newman, J., 1971. Desalting by Means of Porous Carbon Electrodes. J. Electrochem. Soc. 118, 510. https://doi.org/10.1149/1.2408094

Jung, C., Oh, W., Lee, Y., Park, S., 2005. Electrosorption of U ( IV ) by Electochemically Modified Activated Carbon Fibers 6, 25–30.

Kakhi, M., 2009. Classification of the flow regimes in the flow-through cell. Eur. J. Pharm. Sci. 37, 531–544. https://doi.org/10.1016/j.ejps.2009.04.003

Kitous, O., Cheikh, A., Lounici, H., Grib, H., Pauss, A., Mameri, N., 2009. Application of the electrosorption technique to remove Metribuzin pesticide. J. Hazard. Mater. 161, 1035–1039. https://doi.org/10.1016/j.jhazmat.2008.04.091

1371 Koparal, A.S., Yavuz, Y., Bakir Öğütveren, Ü., 2002. Electroadsorption of Acilan Blau Dye
1372 from Textile Effluents by Using Activated Carbon-Perlite Mixtures. Water Environ. Res.
1373 74, 521–525. https://doi.org/10.2175/106143002x140314

1374 Kornyshev, A.A., 2007. Double-Layer in Ionic Liquids: Paradigm Change? J. Phys. Chem. B
1375 111, 5545–5557.

1376 Langlois, S., Coeuret, F., 1990. Flow-through and flow-by porous electrodes of nickel foam
1377 Part III : theoretical electrode potential distribution in the flow-by configuration ~ Mc. J.
1378 Appl. Electrochem. 20, 740–748.

1379 Largeot, C., Portet, C., Chmiola, J., Taberna, P.L., Gogotsi, Y., Simon, P., 2008. Relation
1380 between the ion size and pore size for an electric double-layer capacitor. J. Am. Chem.
1381 Soc. 130, 2730–2731. https://doi.org/10.1021/ja7106178

1382 Le, T.X.H., Bechelany, M., Lacour, S., Oturan, N., Oturan, M.A., Cretin, M., 2015. High
1383 removal efficiency of dye pollutants by electron-Fenton process using a graphene based
1384 cathode. Carbon N. Y. 94, 1003–1011. https://doi.org/10.1016/j.carbon.2015.07.086

1385 Li, Y., Zhang, C., Jiang, Y., Wang, T., Wang, H., 2016. Effects of the hydration ratio on the
1386 electrosorption selectivity of ions during capacitive deionization. DES 399, 171–177.
1387 https://doi.org/10.1016/j.desal.2016.09.011

1388 Li, Z., Shen, C., Liu, Y., Ma, C., Li, F., Yang, B., Huang, M., Wang, Z., Dong, L., Wolfgang,
1389 S., 2020. Carbon nanotube filter functionalized with iron oxychloride for flow-through
1390 electro-Fenton. Appl. Catal. B Environ. 260, 118204.
1391 https://doi.org/10.1016/j.apcatb.2019.118204

1392 Lian, C., Jiang, D.E., Liu, H., Wu, J., 2016. A Generic Model for Electric Double Layers in
1393 Porous Electrodes. J. Phys. Chem. C 120, 8704–8710.
1394 https://doi.org/10.1021/acs.jpcc.6b00964

Lippmann, M.G., 1875. Relations entre les phénomènes électriques et capillaires. Ann. Chim. Phys. 5, 494–549.

Liu, L., Liu, Y., Che, N., Gao, B., Li, C., 2021. Electrochemical adsorption of perfluorooctanoic acid on a novel reduced graphene oxide aerogel loaded with Cu nanoparticles and fluorine. J. Hazard. Mater. 416, 125866. https://doi.org/10.1016/j.jhazmat.2021.125866

López-Bernabeu, S., Ruiz-Rosas, R., Quijada, C., Montilla, F., Morallón, E., 2016. Enhanced removal of 8-quinolinecarboxylic acid in an activated carbon cloth by electroadsorption in aqueous solution. Chemosphere 144, 982–988. https://doi.org/10.1016/j.chemosphere.2015.09.071

Lord, H.L., Zhan, W., Pawliszyn, J., 2012. Fundamentals and Applications of Needle Trap Devices, Comprehensive Sampling and Sample Preparation: Analytical Techniques for Scientists. Elsevier. https://doi.org/10.1016/B978-0-12-381373-2.10056-0

Lust, E., Jänes, A., Lust, K., Pullerits, R., 1997a. Adsorption of organic compounds and hydrophilicity of bismuth, cadmium and antimony electrodes. J. Electroanal. Chem. 431, 183–201. https://doi.org/10.1016/S0022-0728(97)00150-2

Lust, E., Jänes, A., Lust, K., Väärtnõu, M., 1997b. Electric double layer structure and adsorption of cyclohexanol on single crystal cadmium, antimony and bismuth electrodes. Electrochim. Acta 42, 771–783. https://doi.org/10.1016/s0013-4686(96)00339-8

Mantel, T., Jacki, E., Ernst, M., 2021. Electrosorptive removal of organic water constituents by positively charged electrically conductive UF membranes. Water Res. 201, 117318. https://doi.org/10.1016/j.watres.2021.117318

Marracino, J.M., Coeuret, F., Langlois, S., 1987. A first investigation of flow-through porous electrodes made of metallic felts or foams. Electrochim. Acta 32, 1303–1309.

https://doi.org/10.1016/0013-4686(87)85059-4

Martinez-Huitle, C.A., Rodrigo, M.A., Sires, I., Scialdone, O., 2015. Single and coupled electrochemical processes and reactors for the abatement of organic water pollutants : A critical review. Chem. Rev. 115, 13362–13407. https://doi.org/10.1021/acs.chemrev.5b00361

Matsuno, Y., Yoshida, K., Tsutsumi, A., 1996. Electrode performance of fixed and fluidized bed electrodes for a molten carbonate fuel cell anode. Int. J. Hydrogen Energy 21, 663-671.

McGuire, J., Dwiggins, C.F., Fedkiw, P.S., 1985. The electrosorption of phenol onto activated carbon. J. Appl. Electrochem. 15, 53–62. https://doi.org/10.1007/BF00617740

McQuillan, R. V., Stevens, G.W., Mumford, K.A., 2018. The electrochemical regeneration of granular activated carbons: A review. J. Hazard. Mater. 355, 34–49. https://doi.org/10.1016/j.jhazmat.2018.04.079

Monteil, H., Péchaud, Y., Oturan, N., Oturan, M.A., 2019. A review on efficiency and cost effectiveness of electro- and bio-electro-Fenton processes: Application to the treatment of pharmaceutical pollutants in water. Chem. Eng. J. 376, 1–30. https://doi.org/10.1016/j.cej.2018.07.179

Moreira, F.C., Boaventura, R.A.R., Brillas, E., Vilar, V.J.P., 2017. Electrochemical advanced oxidation processes: A review on their application to synthetic and real wastewaters. Appl. Catal. B Environ. 202, 217–261. https://doi.org/10.1016/j.apcatb.2016.08.037

Mousset, E., 2020. Unprecedented reactive electro-mixing reactor: Towards synergy between micro- and macro-reactors? Electrochem. commun. 118, 106787. https://doi.org/10.1016/j.elecom.2020.106787

Mousset, E., Dionysiou, D.D., 2020. Photoelectrochemical reactors for treatment of water and wastewater: a review. Environ. Chem. Lett. 18, 1301–1318. https://doi.org/10.1007/s10311-020-01014-9

Mousset, E., Doudrick, K., 2020. A review of electrochemical reduction processes to treat oxidized contaminants in water. Curr. Opin. Electrochem. 22, 221–227. https://doi.org/10.1016/j.coelec.2020.07.008

Mousset, E., Ko, Z.T., Syafiq, M., Wang, Z., Lefebvre, O., 2016a. Electrocatalytic activity enhancement of a graphene ink-coated carbon cloth cathode for oxidative treatment. Electrochim. Acta. https://doi.org/http://dx.doi.org/10.1016/j.electacta.2016.11.151

Mousset, E., Loh, W.H., Lim, W.S., Jarry, L., Wang, Z., Lefebvre, O., 2021a. Cost comparison of advanced oxidation processes for wastewater treatment using accumulated oxygen-equivalent criteria. Water Res. 200, 117234. https://doi.org/https://doi.org/10.1016/j.electacta.2021.138466

Mousset, E., Oturan, N., Oturan, M.A., 2018a. An unprecedented route of OH radical reactivity evidenced by an electrocatalytical process: Ipso-substitution with perhalogenocarbon compounds. Appl. Catal. B Environ. 226, 135–146. https://doi.org/10.1016/j.apcatb.2017.12.028

Mousset, E., Pechaud, Y., Oturan, N., Oturan, M.A., 2019a. Charge transfer/mass transport competition in advanced hybrid electrocatalytic wastewater treatment: Development of a new current efficiency relation. Appl. Catal. B Environ. 240, 102–111. https://doi.org/10.1016/j.apcatb.2018.08.055

Mousset, E., Pontvianne, S., Pons, M.-N., 2018b. Fate of inorganic nitrogen species under homogeneous Fenton combined with electro-oxidation/reduction treatments in synthetic solutions and reclaimed municipal wastewater. Chemosphere 201, 6–12.

https://doi.org/10.1016/j.chemosphere.2018.02.142

Mousset, E., Puce, M., Pons, M.N., 2019b. Advanced electro-oxidation with boron-doped diamond for acetaminophen removal from real wastewater in a microfluidic reactor: Kinetics and mass-transfer studies. ChemElectroChem 6, 2908–2916. https://doi.org/10.1002/celc.201900182

Mousset, E., Quackenbush, L., Schondek, C., Gerardin-Vergne, A., Pontvianne, S., Kmiotek, S., Pons, M.N., 2020. Effect of homogeneous Fenton combined with electron transfer on the fate of inorganic chlorinated species in synthetic and reclaimed municipal wastewater. Electrochim. Acta 334, 135608. https://doi.org/10.1016/j.electacta.2019.135608

Mousset, E., Trellu, C., Olvera-Vargas, H., Pechaud, Y., Fourcade, F., Oturan, M.A., 2021b. Electrochemical technologies coupled with biological treatments. Curr. Opin. Electrochem. 26, 100668. https://doi.org/10.1016/j.coelec.2020.100668

Mousset, E., Wang, Z., Hammaker, J., Lefebvre, O., 2017. Electrocatalytic phenol degradation by a novel nanostructured carbon fiber brush cathode coated with graphene ink. Electrochim. Acta 258, 607–617. https://doi.org/10.1016/j.electacta.2017.11.104

Mousset, E., Wang, Z., Hammaker, J., Lefebvre, O., 2016b. Physico-chemical properties of pristine graphene and its performance as electrode material for electro-Fenton treatment of wastewater. Electrochim. Acta 214, 217–230. https://doi.org/10.1016/j.electacta.2016.08.002

Mousset, E., Wang, Z., Olvera-Vargas, H., Lefebvre, O., 2018c. Advanced electrocatalytic pre-treatment to improve the biodegradability of real wastewater from the electronics industry — A detailed investigation study. J. Hazard. Mater. 360, 552–559. https://doi.org/10.1016/j.jhazmat.2018.08.023

Nainamalai, M., Palani, M., Soundarajan, B., Allwin, A.E., 2018. Decolorization of synthetic dye wastewater using packed bed electro-adsorption column. Chem. Eng. Process. - Process Intensif. 130, 160–168. https://doi.org/10.1016/j.cep.2018.06.013

Nan, X., Lavrni, S., Toscano, A., 2020. Potential of constructed wetland treatment systems for agricultural wastewater reuse under the EU framework 275. https://doi.org/10.1016/j.jenvman.2020.111219

Newman, J., 1968. Engineering Design of Electrochemical Systems. Ind. Eng. Chem. 60, 12–27. https://doi.org/10.1021/ie50700a005

Newman, J.S., Tobias, C.W., 1962. Theoretical Analysis of Current Distribution in Porous Electrodes. J. Electrochem. Soc. 109, 1183. https://doi.org/10.1149/1.2425269

Nidheesh, P. V., Divyapriya, G., Oturan, N., Trellu, C., Oturan, M.A., 2019. Environmental applications of boron-doped diamond electrodes: 1. Applications in water and wastewater treatment. ChemElectroChem 6, 1–20. https://doi.org/10.1002/celc.201801876

Nie, C., Dai, Z., Meng, H., Duan, X., Qin, Y., Zhou, Y., Ao, Z., Wang, S., An, T., 2019. Peroxydisulfate activation by positively polarized carbocatalyst for enhanced removal of aqueous organic pollutants. Water Res. 166, 115043. https://doi.org/10.1016/j.watres.2019.115043

Niu, J., Conway, B.E., 2003. Adsorption of organics onto an high-area C-cloth electrode from organic solvents and organic solvent/water mixtures. J. Electroanal. Chem. 546, 59–72. https://doi.org/10.1016/S0022-0728(03)00146-3

Norra, G.F., Radjenovic, J., 2021. Removal of persistent organic contaminants from wastewater using a hybrid electrochemical-granular activated carbon (GAC) system. J. Hazard. Mater. 415, 125557. https://doi.org/10.1016/j.jhazmat.2021.125557

1514 Oleinick, A., Svir, I., Amatore, C., 2019. A few key theoretical issues of importance in
1515 modern molecular electrochemistry. Curr. Opin. Electrochem. 13, 33–39.
1516 https://doi.org/10.1016/j.coelec.2018.10.008

1517 Oller, I., Malato, S., Sánchez-Pérez, J.A., 2011. Combination of advanced oxidation processes
1518 and biological treatments for wastewater decontamination-A review. Sci. Total Environ.
1519 409, 4141–4166. https://doi.org/10.1016/j.scitotenv.2010.08.061

1520 Panizza, M., Cerisola, G., 2009. Direct and mediated anodic oxidation of organic pollutants.
1521 Chem. Rev. 109, 6541–6569. https://doi.org/10.1021/cr9001319

1522 Panizza, M., Michaud, P. a., Cerisola, G., Comninellis, C., 2001. Anodic oxidation of 2-
1523 naphthol at boron-doped diamond electrodes. J. Electroanal. Chem. 507, 206–214.
1524 https://doi.org/10.1016/S0022-0728(01)00398-9

1525 Pazos, M., Rosales, E., Sanrom, M.A., 2021. Electro-reversible adsorption as a versatile tool
1526 for the removal of diclofenac from wastewater 280.
1527 https://doi.org/10.1016/j.chemosphere.2021.130778

1528 Pilon, L., Wang, H., d'Entremont, A., 2015. Recent Advances in Continuum Modeling of
1529 Interfacial and Transport Phenomena in Electric Double Layer Capacitors. J.
1530 Electrochem. Soc. 162, A5158–A5178. https://doi.org/10.1149/2.0211505jes

1531 Plaisance, H., Mocho, P., Bonnecaze, G., 1996. Adsorption et electrosorption de benzene sur
1532 charbon actif en grains adsorption and electrosorption of benzene on granular activated
1533 carbon. Environ. Technol. (United Kingdom) 17, 1313–1325.
1534 https://doi.org/10.1080/09593331708616501

1535 Pletcher, D., Walsh, F.C., 1993. Industrial Electrochemistry, Springer Netherlands.
1536 https://doi.org/10.1007/978-94-011-2154-5

1537 Pletcher, D., Walsh, F.C., 1982. Industrial electrochemistry, 1st Ed. ed. Chapman and Hall,
1538 London. https://doi.org/10.1179/bcj.1983.18.2.70

1539 Rezakazemi, M., Maghami, M., Mohammadi, T., 2018. High Loaded Synthetic Hazardous
1540 Wastewater Treatment Using Lab- Scale Submerged Ceramic Membrane Bioreactor 62,
1541 299–304.

1542 Rizzo, L., Gernjak, W., Krzeminski, P., Malato, S., McArdell, C.S., Perez, J.A.S., Schaar, H.,
1543 Fatta-Kassinos, D., 2020. Best available technologies and treatment trains to address
1544 current challenges in urban wastewater reuse for irrigation of crops in EU countries. Sci.
1545 Total Environ. 710, 136312. https://doi.org/10.1016/j.scitotenv.2019.136312

1546 Rong, C., Xien, H., 2009. Reversible electrosorption of thiocyanate anions by active carbon
1547 felt. Sep. Sci. Technol. 44, 3984–3999. https://doi.org/10.1080/01496390903182453

1548 Rong, C., Xien, H., 2005. Electrosorption of thiocyanate anions on active carbon felt
1549 electrode in dilute solution. J. Colloid Interface Sci. 290, 190–195.
1550 https://doi.org/10.1016/j.jcis.2005.04.022

1551 Sahin, E.M., Tongur, T., Ayranci, E., 2020. Removal of azo dyes from aqueous solutions by
1552 adsorption and electrosorption as monitored with in-situ UV-visible spectroscopy. Sep.
1553 Sci. Technol. 55, 3287–3298. https://doi.org/10.1080/01496395.2019.1676786

1554 Schmickler, W., 2020. Double layer theory. J. Solid State Electrochem. 24, 2175–2176.
1555 https://doi.org/10.1007/s10008-020-04597-z

1556 Schmickler, W., 1996. Electronic effects in the electric double layer. Chem. Rev. 96, 3177–
1557 3200. https://doi.org/10.1021/cr940408c

1558 Schultze, J.W., Vetter, K.J., 1973. Experimental determination and interpretation of the
1559 electrosorption valency gamma. Electroanal. Chem. Interfacial Electrochem. 44, 63–81.

Sene, A., Daffos, B., Taberna, P.L., Simon, P., 2019. Characterization of the mass transfer fluxes in a capacitive desalination cell by using FeIII(CN)63−/FeII(CN)64− redox couple as an electrochemical probe. J. Electroanal. Chem. 842, 127–132. https://doi.org/10.1016/j.jelechem.2019.04.060

Simon, P., Gogotsi, Y., 2008. Materials for electrochemical capacitors. Nat. Mater. 7, 845–854.

Stenina, E. V., Baturina, O.A., Sviridova, L.N., Damaskin, B.B., 2001. Coadsorption of halide anions and 1-adamantanol molecules on a mercury electrode. Russ. J. Electrochem. 37, 931–938.

Stenina, E. V., Sviridova, L.N., Damaskin, B.B., 2009. Comparison of temperature dependences of adsorption parameters for secondary butanol and 1-oxyadamantane at their adsorption on the Hg electrode/aqueous solution interface. Russ. J. Electrochem. 45, 847–854. https://doi.org/10.1134/S1023193509080023

Stern, O., 1924. Zur Theorie der Elektrolytischen Doppelschicht. Zeitschrift fur Elektrochemie 30, 508–516.

Storck, A., Vergnes, F., Le Goff, P., 1975. Transfert de matière entre un électrolyte et une paroi cylindrique immergée dans un lit fixe ou fluidisé de grains isolants. Powder Technol. 12, 215–223.

Strohl, J.H., Dunlap, K.L., 1972. Electrosorption and Separation of Quinones on a Column of Graphite Particles. Anal. Chem. 44, 2166–2170. https://doi.org/10.1021/ac60321a012

Su, S.X., Hatton, T.A., 2016. Electrosorption 1. Kirk-Othmer Encycl. Chem. Technol. 1–11. https://doi.org/10.1002/0471238961.koe00022

Su, X., Hatton, T.A., 2017. Electrosorption at functional interfaces: From molecular-level

interactions to electrochemical cell design. Phys. Chem. Chem. Phys. 19, 23570–23584. https://doi.org/10.1039/c7cp02822a

Sun, X.-F., Guo, B.-B., He, L., Xia, P.-F., Shu-Guang Wang, 2016. Electrically Accelerated Removal of Organic Pollutants by a Three-Dimensional Graphene Aerogel. AIChE J. 59, 215–228. https://doi.org/10.1002/aic

Trasatti, S., 1992. Adsorption of organic substances at electrodes: Recent advances. Electrochim. Acta 37, 2137–2144. https://doi.org/10.1016/0013-4686(92)85104-S

Trasatti, S., 1972. Work function, electronegativity, and electrochemical behaviour of metals. III. Electrolytic hydrogen evolution in acid solutions. J. Electroanal. Chem. 39, 163–184. https://doi.org/10.1016/S0022-0728(72)80485-6

Trellu, C., Olvera Vargas, H., Mousset, E., Oturan, N., Oturan, M.A., 2021. Electrochemical technologies for the treatment of pesticides. Curr. Opin. Electrochem. 26, 100677. https://doi.org/10.1016/j.coelec.2020.100677

UNESCO, 2019. The United Nations world water development report 2019: leaving no one behind. UN Educ. Sci. Cult. Organ.

Vafakhah, S., Beiramzadeh, Z., Saeedikhani, M., Ying, H., 2020. A review on free-standing electrodes for energy-e ff ective desalination : Recent advances and perspectives in capacitive deionization. Desalination 493, 114662. https://doi.org/10.1016/j.desal.2020.114662

Varley, C.F., 1871. Polarization of metallic surfaces in aqueous solutions. On a new method of obtaining electricity from mechanical force, and certain relations between electrostatic induction and the decomposition of water. Philos. Trans. R. Soc. London 161, 129–136. https://doi.org/10.1098/rstl.1871.0008

Vetter, K.J., Schultze, J.W., 1974. General Aspects of the Electrosorption Valency. Electroanal. Chem. Interfacial Electrochem. 53, 67–76.

Vilar, E.O., Coeuret, F., 1999. Détermination électrochimique du nombre de sherwood minimum pour un milieu macro-poreux (fritté - Lit fixe de grains). Can. J. Chem. Eng. 77, 855–862. https://doi.org/10.1002/cjce.5450770510

Volfkovich, Y.M., 2020. Capacitive Deionization of Water ( A Review ) 56, 18–51. https://doi.org/10.1134/S1023193520010097

Wadhawan, S., Jain, A., Nayyar, J., Kumar, S., 2020. Journal of Water Process Engineering Role of nanomaterials as adsorbents in heavy metal ion removal from waste water : A review. J. Water Process Eng. 33, 101038. https://doi.org/10.1016/j.jwpe.2019.101038

Waegele, M.M., Gunathunge, C.M., Li, J., Li, X., 2019. How cations affect the electric double layer and the rates and selectivity of electrocatalytic processes. J. Chem. Phys. 151, 1DUMMT. https://doi.org/10.1063/1.5124878

Wagner, C., 1951. Theoretical Analysis of the Current Density Distribution in Electrolytic Cells. J. Electrochem. Soc. 98, 116. https://doi.org/10.1149/1.2778113

Wang, S., Deng, A.N., Wei, J., Guo, Z., Zhang, N., Guo, Z.Y., 2012. Electrosorption-enhanced micro-column solid-phase extraction of traces of cresol red in water using electrodes of stainless steel wire coated with non-conductive polymer. Adsorpt. Sci. Technol. 30, 241–253. https://doi.org/10.1260/0263-6174.30.3.241

Wang, Yujing, Zhao, H., Chai, S., Wang, Yabo, Zhao, G., Li, D., 2013. Electrosorption enhanced electro-Fenton process for efficient mineralization of imidacloprid based on mixed-valence iron oxide composite cathode at neutral pH. Chem. Eng. J. 223, 524–535. https://doi.org/10.1016/j.cej.2013.03.016

Xu, F., Chang, L., Duan, X., Bai, W., Sui, X., Zhao, X., 2019. A novel layer-by-layer CNT/PbO 2 anode for high-efficiency removal of PCP-Na through combining adsorption/electrosorption and electrocatalysis. Electrochim. Acta 300, 53–66. https://doi.org/10.1016/j.electacta.2019.01.090

Yan, J.W., Tian, Z.Q., Mao, B.W., 2017. Molecular-level understanding of electric double layer in ionic liquids. Curr. Opin. Electrochem. 4, 105–111. https://doi.org/10.1016/j.coelec.2017.09.008

Yang, W., Zhou, M., Ma, L., 2021. A continuous flow-through system with integration of electrosorption and peroxi-coagulation for efficient removal of organics. Chemosphere 274, 129983. https://doi.org/10.1016/j.chemosphere.2021.129983

Yao, C., Zhang, W., Xu, L., Cheng, M., Su, Y., Xue, J., Liu, J., Hou, S., 2021. A facile synthesis of porous MXene-based freestanding film and its spectacular electrosorption performance for organic dyes. Sep. Purif. Technol. 263, 118365. https://doi.org/10.1016/j.seppur.2021.118365

Yue, F., Zhang, Q., Xu, L., Zheng, Y., Yao, C., Jia, J., Leng, W., Hou, S., 2019. Porous Reduced Graphene Oxide/Single-Walled Carbon Nanotube Film as Freestanding and Flexible Electrode Materials for Electrosorption of Organic Dye. ACS Appl. Nano Mater. 2, 6258–6267. https://doi.org/10.1021/acsanm.9b01236

Zabasajja, J., Savinell, R.F., 1989. Electrosorption of n- alcohols on graphite particles. AIChE J. 35, 755–763. https://doi.org/10.1002/aic.690350507

Zaharaddeen, S.I., Subramani, C., Dash, S.S., 2016. A Brief Review on Electrode Materials for Supercapacitor. Int. J. Electrochem. Sci. 11, 10628–10643. https://doi.org/10.20964/2016.12.50

Zhang, C., He, D., Ma, J., Tang, W., Waite, T.D., 2018a. Faradaic reactions in capacitive

deionization ( CDI ) - problems and possibilities : A review 128, 314–330. https://doi.org/10.1016/j.watres.2017.10.024

Zhang, C., He, D., Ma, J., Tang, W., Waite, T.D., 2018b. Faradaic reactions in capacitive deionization (CDI) - problems and possibilities: A review. Water Res. 128, 314–330. https://doi.org/10.1016/j.watres.2017.10.024

Zhang, W., Liu, N., Cao, Y., Lin, X., Liu, Y., Feng, L., 2017. Superwetting Porous Materials for Wastewater Treatment : from Immiscible Oil / Water Mixture to Emulsion Separation. Adv. Mater. Interfaces 4(10). https://doi.org/10.1002/admi.201700029